NBSIR 76-1108

Fabrication of the Barium Fluoride Film Humidity Sensor by Industrial Firms

Frank E. Jones

Heat Division
Institute for Basic Standards
National Bureau of Standards
Washington, D.C. 20234

April 1977

Final

Prepared for

Cambridge Air Force Geophysical Laboratories
Department of the Air Force
Hanscom Air Force Base
Bedford, Massachusetts 01731

NBSIR 76-1108

FABRICATION OF THE BARIUM FLUORIDE FILM HUMIDITY SENSOR BY INDUSTRIAL FIRMS

Frank E. Jones

Heat Division
Institute for Basic Standards
National Bureau of Standards
Washington, D.C. 20234

April 1977

Final

Prepared for
Cambridge Air Force Geophysical Laboratories
Department of the Air Force
Hanscom Air Force Base
Bedford, Massachusetts 01731

U.S. DEPARTMENT OF COMMERCE, Juanita M. Kreps, *Secretary*

Dr. Betsy Ancker-Johnson, *Assistant Secretary for Science and Technology*

NATIONAL BUREAU OF STANDARDS, Ernest Ambler, *Acting Director*

ABSTRACT

The barium fluoride film electric hygrometer element, which was conceived and developed at the National Bureau of Standards as a fast responding humidity sensor and which has been used in a variety of research applications, has been successfully fabricated by several commercial firms. This successful transfer of technology from the Federal Government to the private sector should assure the availability of the element for general use, including missile climatology and routine radiosonde use. Calibration equations have been developed and the analysis of calibration data has provided insight into the physical processes involved in the functioning of the element.

It has been shown that the conductance - $\frac{p}{p_s}$ isotherm (in itself a Type II isotherm in the Brunauer designation of physical adsorption isotherms) is a composite of a Type I and two Type III isotherms. The two Type III isotherm equations are of the form of the Freundlich isotherm equation. These results represent the solution of a long-standing problem in adsorption and have general application to other adsorption systems in addition to the water vapor-barium fluoride film system.

Key Words: Barium fluoride; calibration equations; fast response; films; humidity sensor; industrial fabrication; isotherm equations; physical adsorption; relative humidity; routine radiosonde application.

CONTENTS

1. INTRODUCTION

The barium fluoride film electric hygrometer element [1,2] was developed as a fast responding radiosonde humidity sensor. A series of radiosonde flights [3] established the capability of the element for radiosonde use on an experimental basis; however, the instability of the element with time, as indicated by an observable shift in calibration in a period as short as one day, precluded its use in routine radiosonde flights at that state of its development. A study of the aging characteristics of the element and of possible causes of the drift of calibration with time led to changes in fabrication procedures which substantially improved the stability of the element [4].

The rapid response of the element to rapid changes or fluctuations of humidity [5] make it a valuable research tool. The element has been used in a field study of the effectiveness of monomolecular films of alcohol mixtures for reducing evaporation of water from a lake [6], for measurements, by an eddy correlation method, of evaporation from a crop surface [7], mounted in a probe on an aircraft to determine the horizontal profiles of humidity through fair weather clouds [8], and in a laboratory determination of the humidity distribution with height above a free water surface [9]. These successful applications established the suitability of the element for a variety of meteorological applications that require detailed moisture fluctuation information, e.g., as an improved radiosonde element for general application and for particular application at missile test ranges.

In order to make the element generally available for various applications, it was one of the objectives of the present work to develop commercial sources of the element, i.e., to transfer the fabrication technology to the private sector and to determine whether there are firms with the capability of producing barium fluoride film electric hygrometer elements which exhibit a performance that is equivalent to (or better than) the performance of those developed and fabricated at NBS. The procurement and calibration of a number of commercially-produced barium fluoride elements was the other objective of the present work.

The barium fluoride film electric hygrometer element, illustrated in figure 1, consists of a glass substrate on which a film of barium fluoride, 0.3 μm thick, has been deposited by vapor deposition over closely-spaced metallic film electrodes.

The production of a barium fluoride film element consists of two separable operations: 1) the fabrication of the metallic film electrode pattern on the substrate and 2) the deposition of the barium fluoride film over the electrode pattern. In the development of the element at NBS both operations were devised and performed (2),therefore, a potential commercial supplier with competence in the deposition of thin films could be expected to be capable of performing both operations. However, it was considered for the present work to be more effective and efficient to attempt to locate two categories of suppliers: 1) those who could supply the substrates with electrode patterns and 2) those who could deposit the barium fluoride films. The second of these operation is by far the more critical.

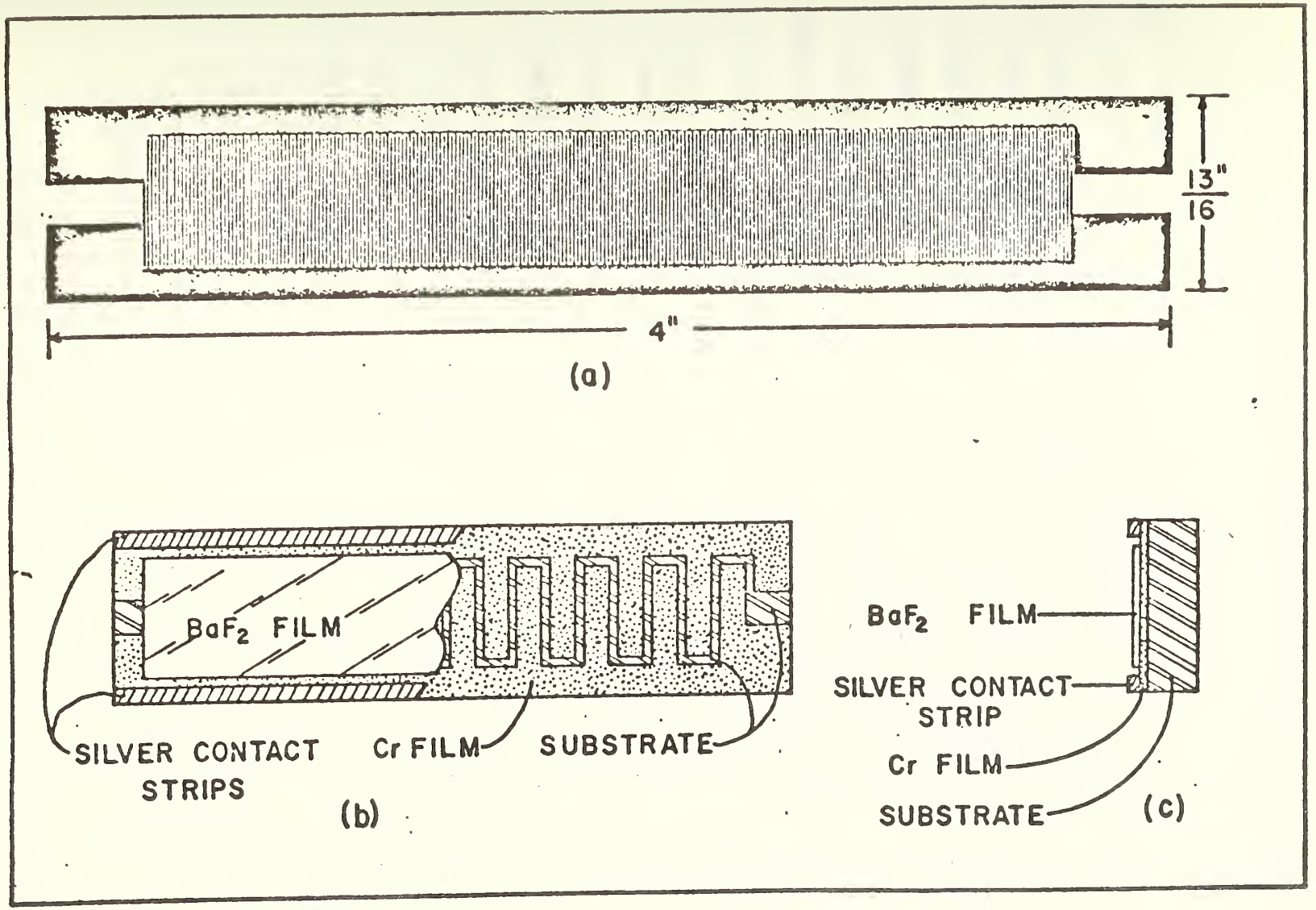

FIGURE 1. Barium fluoride film electric hygrometer element construction and electrode configuration.

2. COMMERCIAL SUPPLIERS OF ELECTRODE PATTERNS AND BARIUM FLUORIDE FILMS.

Two suppliers were located who could and did produce satisfactory electrode patterns by photoetching chromium film covered masking plates; these suppliers were the sources of all of the substrates with electrode patterns which were used for the deposition of the barium fluoride films. Five firms were invited to deposit the barium fluoride films on a limited number of substrates by the procedures described in references 2 and 4.

The procedures developed at NBS, described in references 2 and 4, will be briefly outlined here in the interest of completeness. After the electrode patterns were formed by the electro-etching process, the substrates were cleaned by a detergent-and-water wash followed by rinses in distilled water, in isopropyl alcohol and a vapor degreasing in an isopropyl alcohol degreaser. The substrates were then placed, electrode face down, on a support in the bell jar of an oil diffusion-pumped vacuum evaporator. The source used for the deposition of the barium fluoride film was a solid mass of barium fluoride, formed by vacuum melting and subsequent cooling of reagent-grade barium fluoride powder, in a molybdenum "boat." A junction of a platinum, platinum-rhodium thermocouple was embedded in the solid mass. A glow discharge was maintained for approximately 20 minutes, after which the pressure was lowered to approximately 5×10^{-5} Torr. The barium fluoride charge, covered by a tantalum baffle, was heated until the thermocouple indication was 1160°C. The baffle was then removed for 5 minutes, during which time the barium fluoride deposited on the substrates. During the deposition, the electrical power to the "boat" was adjusted

to maintain the 1160°C temperature indication. The thickness of the barium fluoride film was determined interferometrically to be 0.3 micrometer. The construction of the finished element is shown in figure 1. The results of various experiments described in reference 4 and the considerations therein indicated the possibility that contamination by diffusion pumping fluid was a source of the previously observed drift of the calibration of the barium fluoride film element. Therefore, the production procedures were modified as follows: 1) liquid nitrogen was maintained in both the mechanical pump cold trap and the oil diffusion pump trap throughout the production process; 2) the distance between the evaporation source and the substrates was reduced from 38 cm to 19 cm; 3) the substrates were exposed to a glow discharge for approximately 76 minutes during which time the substrate temperature increased to approximately 160°C. The glow discharge was produced by an electrode assembly designed to expose the substrates to positive species in the discharge and to reduce if not eliminate electron bombardment; 4) the deposition was started within 3 minutes after the glow discharge power supply was turned off; 5) the time of deposition was reduced from 300 sec to 180 sec; and 6) argon was introduced into the evaporator as soon as possible after the deposition of the film to bring the pressure to ambient in the relative absence of oxygen. The pumping fluid in the diffusion pump was DC705 silicone and the bell jar gasket was made of Viton.

The five suppliers of the barium fluoride films were provided with copies of references 2 and 4 and asked to follow these procedures. However, the availability of electron bombardment heating apparatus and optical film thickness monitoring and control apparatus and other refinements enabled the individual suppliers to depart from these procedures without potential deleterious effects on the performance of the finished elements.

3. ROOM TEMPERATURE CALIBRATION

The performance of the completed barium fluoride film electric hygrometer elements as received from the five firms which deposited the barium fluoride films was first investigated by performing room temperature calibrations of the elements. The calibrations consist of measurement of the electrical resistance of the elements at a series of relative humidity (RH) points. The goal of the calibration was to determine whether the performance of elements produced by commerical suppliers was comparable to or better than that of those produced at NBS. Prior to the calibration, the elements were subjected to a heat treatment which had in earlier work resulted in considerable reduction in element resistance at room temperature [2] and which had in later work [4] been shown to be effective in reversing the effect of "aging" on the calibration of the elements. The heat treatment consisted of raising the temperature of the elements to temperatures in the range of 350°C to 400°C in a furnace for 1 hour then slowly returning the elements to room temperature (usually overnight).

The elements were then exposed to 6 cycles of relative humidity, RH, between near 0% RH (over barium oxide desiccant) and near 100% RH (over distilled water), exposure at each RH was for 10 minutes. The elements were then immediately passed through a series of RH points established by saturated salt solutions in sealed glass jars; the elements were maintained at each RH for 20 minutes. The sequence of RH was one of alternation between high and low RH's, for example: 100, 29, 97, 33.5%, etc.

The calibration RH's and the salts used to establish them were: 12%, lithium chloride (LiCl); 29%, calcium chloride ($CaCl_2$); 33.5%, magnesium chloride ($MgCl_2 \cdot 6H_2O$); 38.5%, sodium iodide (NaI); 48.5%, lithium nitrate ($LiNO_3$); 53.5%, magnesium nitrate ($Mg(NO_3)_2 \cdot 6H_2O$); 64.5%, sodium nitrite ($NaNO_2$); 71.0%, strontium chloride ($Sr\ Cl_2 \cdot 6H_2O$); 75.5%, sodium chloride (NaCl); 80.5%, potassium bromide (KBr); 84.5%, potassium chloride (KCl); 87.0%, zinc sulfate ($ZnSO_4 \cdot 7H_2O$); 90.5%, barium chloride ($BaCl_2 \cdot 2H_2O$); 92.0%, potassium nitrate (KNO_3) and 97.0%, potassium sulfate (K_2SO_4).

The electronic circuitry used for the room temperature calibration had been designed by R. Bruce Uhlenhopp and was of the type used in several research applications of the element [5,6,8,9]. The circuit was calibrated using resistance boxes and the output was measured using a digital voltmeter. The room temperature calibrations were performed on elements from four suppliers, A, B, C and D, on four successive Saturdays. These four sessions of calibration made it possible to calibrate a number of elements from each of the four suppliers and also to provide information on the short-term stability of some of the elements.

On 9/6/75 four elements from each of three suppliers, designated A, B, and C, were calibrated at a room temperature of 25°C and a room RH of 49%. The elements from supplier C were found to be unsatisfactory presumably due to exposure of the substrates to electron bombardment during the glow discharge bombardment prior to deposition of the barium fluoride film [4], and were eliminated from further investigation. On 9/13/75 the elements from supplier C were replaced by four additional elements from supplier B; these, with the four elements each from suppliers A and B calibrated on 9/6/75 were calibrated at room temperature. On 9/20/75 the second set of elements from supplier B was replaced by four elements from supplier D; these, with the others calibrated on 9/6/75 and 9/13/75 were calibrated at room temperature. On 9/27/75, due to the limited capacity for calibrating elements, the set of four elements from supplier D was replaced by the four elements from supplier B which were replaced on 9/20/75 and reheated on 9/26/75; these, with the others calibrated on 9/6/75 and 9/13/75 were calibrated at room temperature.

On 4/26/76, three elements from supplier E were calibrated at room temperature. The elements had been heated for 1 hour in Feb. 1976, and remained in the muffle furnace at room temperature until they were removed on 4/21/76. The RH cycling of the elements was performed on 4/26/76 before the calibration was made.

The calibration data (element resistance vs relative humidity) for one element from supplier A are plotted in figure 2. The points for the four successive weeks are indicated by different symbols. The data for the remaining three elements from supplier A and for four elements each from suppliers B, D and E are plotted in figures A-1 through A-14 in Appendix A. (Figures not interleaved with the text are presented in Appendix A and

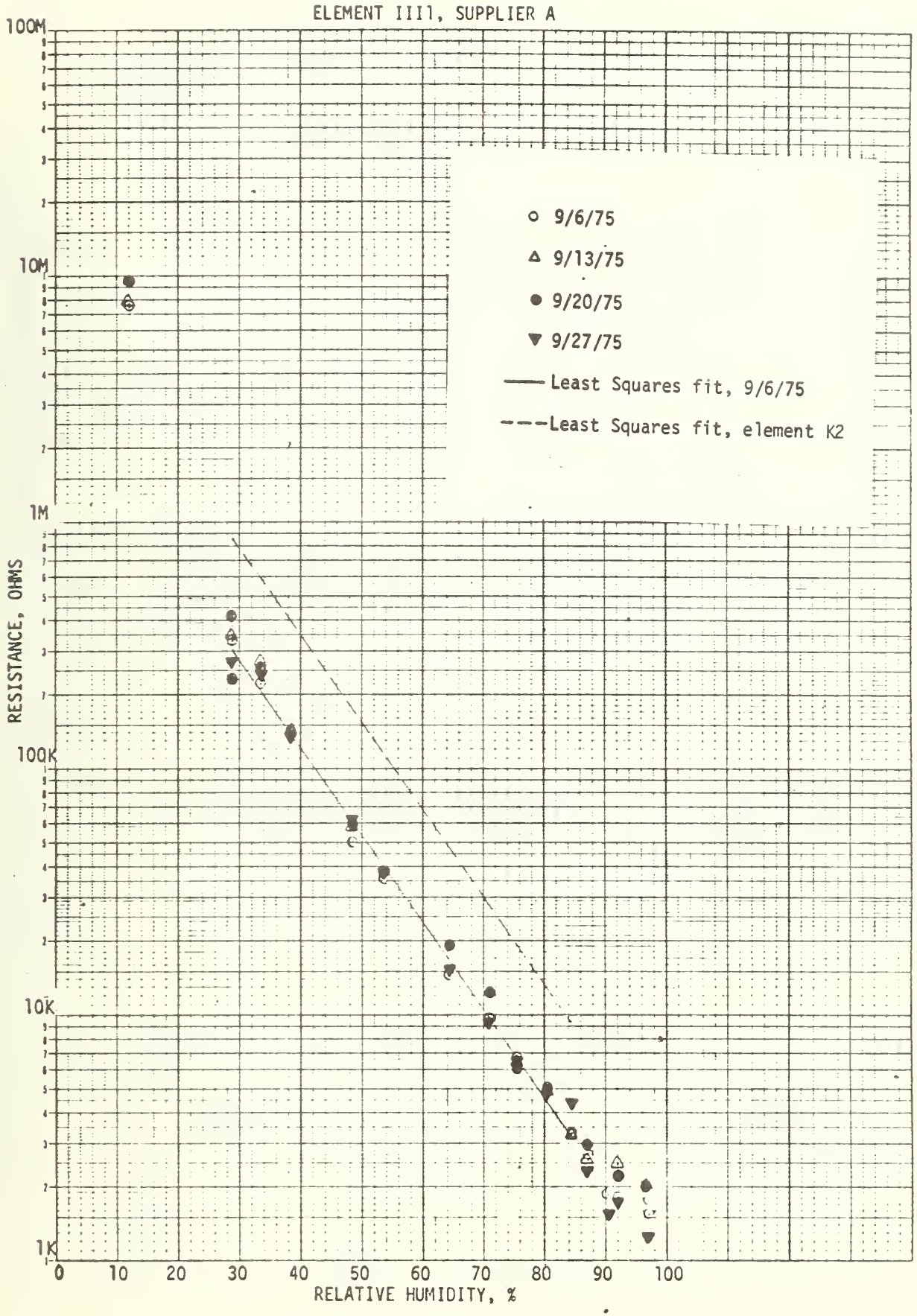

FIGURE 2. Room temperature calibration, element IIII, supplier A.

are designated by the prefix A- with the number). Due to erratic measurements, only six data points (closed circles) are available for element III 3-E.

In previous work at NBS on barium fluoride elements [9] it was found that the room temperature calibration data when plotted as logarithm of the number of ohms of element resistance against relative humidity, separated into three distinct regions. This is illustrated in figure 3. As seen in the figure, the plot is curvilinear in Region I covering the range "0" to 26% RH. In Region II covering the range 26 to 84.5% RH and Region III covering the range 84.5% to 100% RH, the plot is linear. In order to ascertain whether the characteristic shape of the calibration curves for the conimerically manufactured elements was similar to that for the elements produced at NBS, the calibration data in the present work was plotted as shown in figure 2 and a straight line was fitted to the data in Region II. The data for 9/6/75 calibration of the A and B elements, for the 9/20/75 calibration of the D elements and for the 4/26/76 calibration of the E elements have been fitted in the region 29 to 84.5% RH by an equation of the form

$$\ln R = a = b\ RH \qquad (1)$$

by the method of least squares, where ln R is the natural (Naperian) logarithm of the number of ohms of resistance of the element. The straight solid line in the figures is the plot of equation 1. For comparison, the dashed line is a plot of a similar equation for an element produced at NBS (element K2 of reference 9).

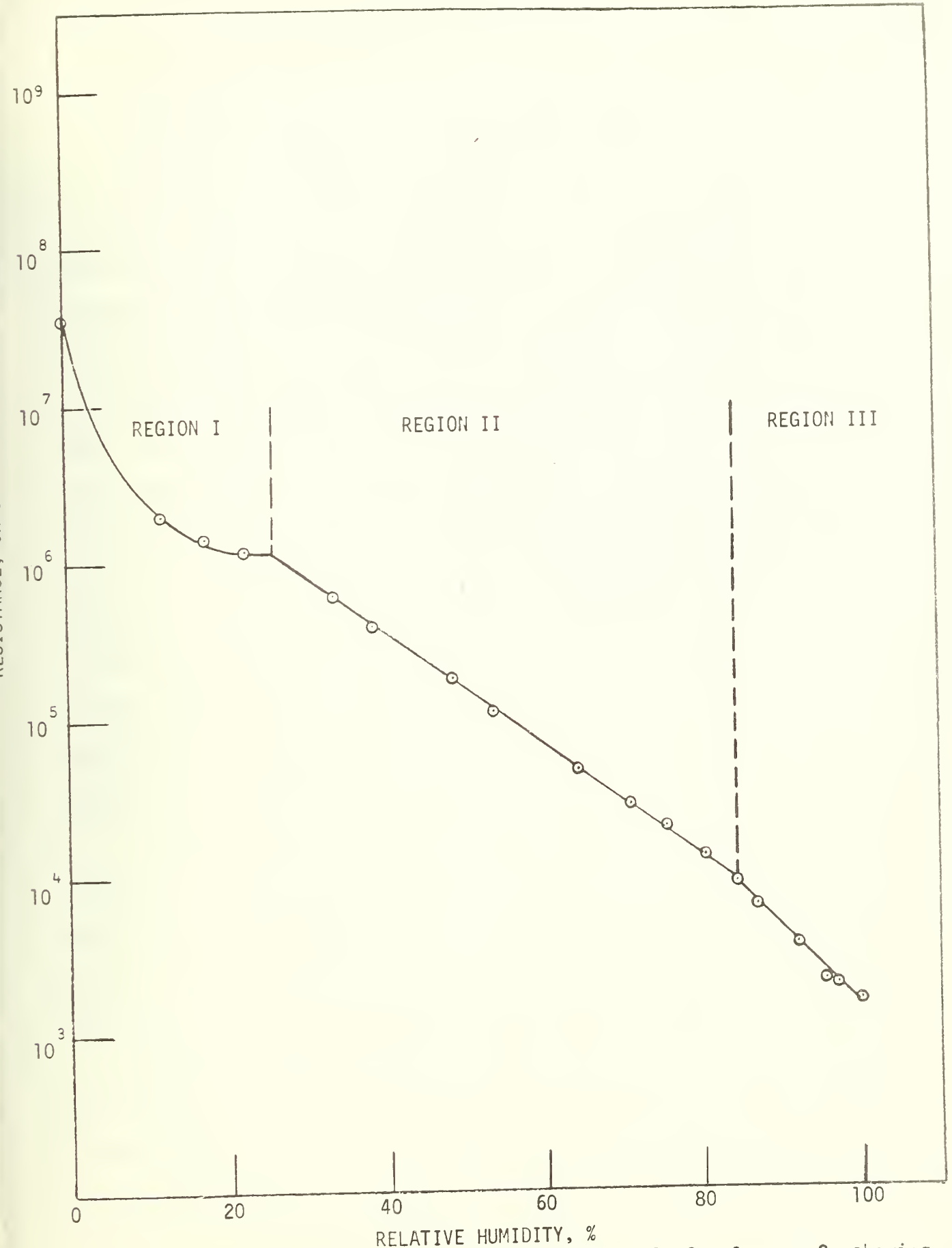

FIGURE 3. Room temperature calibration of element K2 of reference 9, showing separation into three regions.

Although the room temperature calibrations in the present work were made over the range 12 to 97%, there were very little data at the 12% point since the circuitry was not calibrated for resistance higher than 11 megohms. Also, since "shorting strips" (metallic strips painted on or soldered to the electrode films) were not applied to the elements, the resistances included the series resistance of the electrode film and therefore at the high RH's (in the range above approximately 90% RH) the resistance did not represent the optimum performance of the elements. Therefore, the region chosen for assessment of the room temperature performance of the elements was that region, 29 to 84.5% RH, in which earlier work [9] has shown that equation 1 applies.

3.1 Calibration Equations

3.1.1 Development of Equation Relating Element Conductance, G, to Relative Pressure of Water Vapor, $\frac{p}{p_s}$

In this section an empirical equation relating the electrical conductance, $G = \frac{1}{R}$, to the relative pressure of water vapor, $\frac{p}{p_s} = \frac{RH}{100}$, will be developed. Conductance rather than resistance has been chosen to represent the performance of the element since the physics of the situation relates conductance to relative pressure. That is, in the model adopted here water is adsorbed in the BaF_2 film and the mobility of current carriers in the water increases with the "amount" of water adsorbed. The "amount" of water adsorbed and, therefore, the conductance of the BaF_2 film, increases with increasing RH. A plot of conductance versus RH or $\frac{p}{p_s}$ is similar in shape to a typical adsorption isotherm of Type II in the Brunauer designation [12]. In the present treatment the data for BaF_2 films in reference 9 will be reanalyzed to develop a new empirical equation relating G to $\frac{p}{p_s}$ and to relate the terms in the equation to conventional isotherm equations, if possible.

It was shown in reference 9 that the room temperature calibration for barium film elements, when plotted on semilogarithmic graph paper, separates into three distinct regions. This separation is illustrated in figure 3 in which the room temperature data for element K2 of the earlier work are plotted.

In this analytical development, the appearance of three regions is considered to indicate the existence of three different modes of adsorption of water vapor (or of three different types of adsorption sites). The conductance in region I is considered to represent the sum of the zero $\frac{p}{p_s}$

conductance and the conductance due to mode I. In region II, the adsorption mode of region I is considered to be present in addition to a second mode; the conductance thus being the sum of that due to the two modes. Similarly, in region III modes I and II are considered to be present in addition to a third mode, III; the conductance thus being the sum of that due to the three modes. Analytically then, one might expect the relationship between element conductance, G, and relative pressure, $\frac{p}{p_s}$, to be represented by an equation containing a constant term and three terms involving $\frac{p}{p_s}$.

The development of the empirical equation relating element conductance G to relative water vapor pressure, $\frac{p}{p_s}$, will be illustrated by the use of the +23°C room temperature calibration data for element K2 in reference 9. The data are tabulated in table 1 in which the units of conductance G are micromhos [1 micromho = $(\frac{1}{10^6 \text{ ohms}})$].

In order to develop an equation relating G to $\frac{p}{p_s}$, the plot of the calibration data is decomposed into three parts. In regions II and III the data are represented by equations of the form

$$\ln G = \alpha + \beta \frac{p}{p_s} . \qquad (2)$$

Using the method of least squares on the data for region II ($\frac{p}{p_s}$ = 0.335 to 0.805), values α_{II} = -2.14609 and β_{II} = +8.00790 result. Equation 2 thus becomes

$$\ln G_{II} = -2.14609 + 8.00790 \frac{p}{p_s} . \qquad (3)$$

Table 1. Room Temperature, 23°C, Calibration Data for Element K2[1] from Reference 9.

$\frac{p}{p_s} \equiv \frac{RH}{100}$	Conductance, G, in micromhos
0.120	0.500
0.175	0.714
0.225	0.855
0.335	1.61
0.385	2.56
0.485	5.35
0.535	8.70
0.645	21.1
0.710	36.4
0.755	48.8
0.805	75.2
0.845	108
0.870	152
0.920	270
0.955	465
0.970	513

[1] The data for element K2 in reference 9 in the region $\frac{p}{p_s}$ = 0.335 to 0.845 are fitted by the equation: $\ln G = -2.22161 + 8.12993 \frac{p}{p_s}$.

Rearranging equation 3,

$$\frac{p}{p_s} = 0.26800 + 0.12488 \ln G_{II} \tag{4}$$

The values of G_{II} and $\frac{p}{p_s}$ calculated using equations 3 and 4, respectively, are tabulated in table A-1 in Appendix A. (Tables not interleaved with the text are presented in Appendix A and are designated by the prefix A- before the number).

Using the method of least squares on the data for region III ($\frac{p}{p_s}$ = 0.845 to 0.970), values α_{III} = -6.02090 and β_{III} = 12.67352 result. Equation 2 thus becomes

$$\ln G_{III} = -6.02090 + 12.67352 \frac{p}{p_s} . \tag{5}$$

Rearranging equation 5,

$$\frac{p}{p_s} = 0.47508 + 0.078905 \ln G_{III}. \tag{6}$$

The values of G_{III} and $\frac{p}{p_s}$ calculated using equations 5 and 6, respectively, are tabulated in table A-2.

Setting equation 3 equal to equation 5, the point of intersection of the straight line segments for regions II and III can be calculated:

$$-2.14609 + 8.00790 \frac{p}{p_s} = -6.02090 + 12.67352 \frac{p}{p_s} , \tag{7}$$

$$3.87481 = 4.66562 \frac{p}{p_s} , \tag{8}$$

$$\frac{p}{p_s} = 0.831.$$

Recalling that it has been hypothesized that the "measured" conductance, G_{III}, in region III is the sum of the conductances due to three adsorption modes, that the "measured" conductance G_{II} in region II is the sum of conductances due to two of the adsorption modes and that conductances in parallel are additive, the conductance due to mode III is equal to the difference between the conductances calculated from equations 3 and 5, i.e., calc. G_{III} - calc. G_{II}. In table A-3 this difference, designated G_3, is tabulated.

The data for G_3 can be represented by

$$\ln G_3 = c + d \ln \frac{p}{p_s} . \qquad (9)$$

Using the method of least squares, values c = 6.44573 and d = 24.99003 result. Equation 9 thus becomes

$$\ln G_3 = 6.44573 + 24.99003 \ln \frac{p}{p_s} . \qquad (10)$$

Rearranging equation 10,

$$\ln \frac{p}{p_s} = -0.25793 + 0.04002 \ln G_3. \qquad (11)$$

Values of G_3 and $\frac{p}{p_s}$ calculated from equations 10 and 11, respectively, are tabulated in table A-4.

The conductance for region I, i.e., for $\frac{p}{p_s}$ = 0.120, 0.175 and 0.225, is essentially linear with $\ln \frac{p}{p_s}$ and can, therefore, be represented by an

equation of the form

$$\ln \frac{p}{p_s} = f + h\ G_I, \tag{12}$$

where G_I is the "measured" conductance in region I. Using the method of least squares, the values f = -3.00574 and h = +1.77011 result. Thus, equation 12 becomes

$$\ln \frac{p}{p_s} = -3.00574 + 1.77011\ G_I. \tag{13}$$

Rearranging equation 13,

$$G_I = 1.69805 + 0.56494 \ln \frac{p}{p_s}. \tag{14}$$

Values of G_I and $\frac{p}{p_s}$ calculated from equation 14 and 13, respectively, are tabulated in table A-5.

Again, recalling that it has been hypothesized that the conductance G_{II} in region II is the sum of the conductances due to two of the adsorption modes, the conductance G_2 due to mode II is equal to the difference between the conductances calculated from equations 3 and 14, i.e., calc. G_{II} - calc. G_I. In table A-6 this difference, designated G_2, is tabulated. The relationship between G_2 and $\frac{p}{p_s}$ in region II ($\frac{p}{p_s}$ = 0.335 to 0.805) can be represented by an equation of the form

$$\ln G_2 = k + m \ln \frac{p}{p_s}. \tag{15}$$

Using the method of least squares, the values k = 5.34400 and m = 5.31462 result. Thus, equation 15 becomes

$$\ln G_2 = 5.34400 + 5.31462 \ln \frac{p}{p_s} . \qquad (16)$$

Values of G_2 calculated from equation 16 are included in table A-6. The sums of the calculated values of G_I and G_2 are tabulated in table A-7.

It is seen in table A-7 that the sum of G_I and G_2 exceeds G, the "measured" conductance, in region I. This is due to the fact that the "measured" conductance, G_I, in region I was used as a first estimate of the conductance, G_I, due to mode I and as such included some conductance due to mode II. Therefore, new estimates of G_I, designated G_1', were made by reducing G_I by the values calculated for G_2 in region I; thus, the values of G_I' are: 0.500-0.003 = 0.497, 0.714-0.020 = 0.694, and 0.855-0.076 = 0.779. The equation resulting from the treatment of the new estimates, G_1', by the method of least squares is

$$G_1' = 1.46774 + 0.45439 \ln \frac{p}{p_s} . \qquad (17)$$

Values of G_1' calculated from equation 17 are tabulated in table A-8. The difference between G_1' and the calculated values of G_{II}, designated G_2', is also tabulated in table A-8.

The equation resulting from the least squares treatment of G_2' is

$$\ln G_2' = 5.29292 + 5.15798 \ln \frac{p}{p_s} . \qquad (18)$$

The values of G_2' calculated from equation 18 are tabulated in table A-8.

The sum of G_1' and G_2', calculated from equations 17 and 18, respectively, are tabulated in table A-9 for region III ($\frac{p}{p_s}$ = 0.845 to 0.970). This sum subtracted from the "measured" values G is designated G_3' and tabulated in table A-9. The equation resulting from the least squares treatment of G_3' is

$$\ln G_3' = 6.53675 + 19.38125 \ln \frac{p}{p_s} . \qquad (19)$$

Recapitulating, equations have been developed relating the room temperature conductance, $G=(\frac{1}{\text{resistance}})$, for element K2 of reference 9 to the relative pressure of water vapor, $\frac{p}{p_s} = \frac{RH}{100}$. In the region $\frac{p}{p_s}$ = 0.12 to 0.225, equation 17 applies, in the region $\frac{p}{p_s}$ = 0.335 to 0.805, equation 18 applies; and in the region $\frac{p}{p_s}$ = 0.845 to 0.970, equation 19 applies. These three equations represent a decomposition of the plot of G against $\frac{p}{p_s}$. To reconstruct the plot then it is necessary only to combine the three equations. The combined equation is the sum of the three equations, since conductances in series are additive.

The combined equation is

$$G' = G_1' + G_2' + G_3', \qquad (20)$$

where G_1' is given by equation 17, G_2' is found by solving equation 18, and G_3' is found by solving equation 19, viz.:

$$G_1' = 1.46774 + 0.45439 \ln \frac{p}{p_s}, \tag{17}$$

$$G_2' = \exp\left[5.29292 + 5.15798 \ln \frac{p}{p_s}\right],$$

$$G_2' = 198.923 \left(\frac{p}{p_s}\right)^{5.15798} \tag{21}$$

$$G_3' = \exp\left[6.53675 + 19.38125 \ln \frac{p}{p_s}\right]$$

$$G_3' = 690.040 \left(\frac{p}{p_s}\right)^{19.38125} \tag{22}$$

Combining equations 17, 21 and 22,

$$G' = 1.46774 + 0.45439 \ln \frac{p}{p_s} + 198.923 \left(\frac{p}{p_s}\right)^{5.15798} + 690.040 \left(\frac{p}{p_s}\right)^{19.38125}. \tag{23}$$

Substituting the calibration values of $\frac{p}{p_s}$ in equation 23, the calculated values G' are tabulated in table 2 and compared to the "measured" values of G.

3.1.2 Development of Calibration Equations Relating Element Resistance to Relative Humidity.

Having developed an equation relating element conductance to relative pressure of water vapor in the preceding section, we now turn to the development of the conventional form of calibration equations relating element resistance to relative humidity.

We return now to equations 3 and 5,

$$\ln G_{II} = -2.14609 + 8.00790 \frac{p}{p_s}, \tag{3}$$

Table 2. Comparison of the Values of G', Calculated Using Equation 23, and "Measured" Values of G.

	(1) calc. G'_1, in micromhos	(2) calc. G'_2, in micromhos	(3) calc. G'_3, in micromhos	(4) $G'=(1)+(2)+(3)$, in micromhos	(5) G (measured) in micromhos	$\frac{(4)}{(5)}$	$\frac{p}{p_s}$
↑ Region I ↓	0.504	0.004	0.000	0.508	0.500	1.016	0.120
	0.676	0.025	0.000	0.701	0.714	0.982	0.175
	0.790	0.091	0.000	0.881	0.855	1.030	0.225
↑	0.971	0.706	0.000	1.677	1.61	1.042	0.335
	1.034	1.447	0.000	2.481	2.56	0.969	0.385
	1.139	4.762	0.001	5.902	5.35	1.103	0.485
Region II	1.184	7.898	0.004	9.086	8.70	1.044	0.535
↓	1.268	20.720	0.141	22.129	21.1	1.049	0.645
	1.312	34.000	0.904	36.216	36.4	0.995	0.710
	1.340	46.681	2.974	50.995	48.8	1.045	0.755
	1.369	64.980	10.306	76.655	75.2	1.019	0.805
↑	1.391	83.448	26.380	111.219	108	1.039	0.845
	1.404	96.990	46.418	144.812	152	0.953	0.870
Region III	1.430	129.391	137.100	267.921	270	0.992	0.920
↓	1.447	156.871	282.693	441.011	465	0.948	0.955
	1.454	170.002	382.379	553.835	513	1.080	0.970

and

$$\ln G_{II} = -6.02090 + 12.67352 \frac{p}{p_s}, \quad (5)$$

representing the two linear segments of the plot of conductance, G, against relative pressure of water vapor, $\frac{p}{p_s}$. These equations can be changed to represent the relationship between the common logarithm, log, (i.e., logarithm to the base 10) of resistance, R, and relative humidity, RH. Noting first that

$$\ln G_{II} = - \ln R_{II},$$

$$\ln R_{II} = 2.14609 - 8.00790 \frac{p}{p_s}. \quad (24)$$

Noting next that

$$\log R_{II} = \frac{1}{2.30259} \ln R_{II},$$

$$\log R_{II} = 0.93203 - 3.47778 \frac{p}{p_s}. \quad (25)$$

Noting then that $\frac{p}{p_s} = \frac{RH}{100}$,

$$\log R_{II} = 0.93203 - 0.034778 \text{ RH}, \quad (26)$$

where R_{II} is in megohms. Similarly, equation 5 becomes

$$\log R_{III} = 2.61484 - 0.055040 \text{ RH}. \quad (27)$$

If desired in the application of the element, the plot for the region covered by the linear segments, that is, from 24.5 percent to 97 percent RH,

can be linearized, that is, equation 26 can be made to apply to the entire region, by adding a resistance in series with the element. In the case of element K2 from reference 9 the series resistor would be about 1800 ohms.

To estimate the lower limit for the region of applicability of equation 25, and therefore, that region extended by adding the series resistor, the conductance calculated from equations 3 and 14 are set equal and $\frac{p}{p_s}$ is solved for. The lower limit is estimated to be $\frac{p}{p_s} = 0.245$. Therefore, the linearized plot should apply to the RH region 24.5% to 97.0% (and, presumably to 100%).

In region I (from $\frac{p}{p_s} \cong 0$ to $\frac{p}{p_s} \cong 0.245$), the relationship between "measured" conductance G_I and $\frac{p}{p_s}$ is represented by equation 12,

$$\ln \frac{p}{p_s} = f + h\, G_I. \qquad (12)$$

Substituting RH for $\frac{p}{p_s}$ and $\frac{1}{R_I}$ for G_1 and the values determined for f and h, equation 12 becomes

$$\log RH = 0.69463 + \frac{0.76875}{R_I}. \qquad (28)$$

Taking the common logarithm of both sides of equation 28, the following equation results,

$$\log \log \left(\frac{RH}{4.95028}\right) = - 0.11421 - \log R_I. \qquad (29)$$

The relative humidity corresponding to an element resistance of R_I could be found from a plot of either log RH versus $\frac{1}{R_I}$ (where R_I is megohms)

or log log $\left(\frac{RH}{4.95208}\right)$ versus log R_I.

Equations 26, 27, and 28 or 29 are of the forms of element calibration equations. The values of the parameters in the equations for elements produced elsewhere depend upon the capability of the manufacturer of the elements to produce elements typical of those produced at NBS.

3.2 Low Temperature Calibrations

Twenty elements, supplied by three of the suppliers, were calibrated in the NBS Pressure Humidity Apparatus [10] at 25.5, 0.7, -19.3 and -39.3°C. The performance of two of the elements is illustrated in figures 4 and 5. Because of the demonstrated inadequacy of the circuitry used for measuring element resistance in this series of calibrations, particularly at low temperatures, and because of other uncertainties caused by the lack of information on its performance, it is not possible to derive reliable quantitative information. However, it can be observed that the elements responded to changes in RH at temperatures as low as -39.3°C, the lowest in the calibration series; straight lines on the plots of logarithm of resistance vs relative humidity appear to represent the data over the range about 30 to 80% RH for temperatures down to -19.3°C; the straight lines for the several temperatures tend to be parallel and the resistance at a given RH increases with decreasing temperature. The treatment in reference 9 in which the temperature dependence of the resistance is assigned to the intercept of the straight line plot appears to be valid for the data in this calibration series.

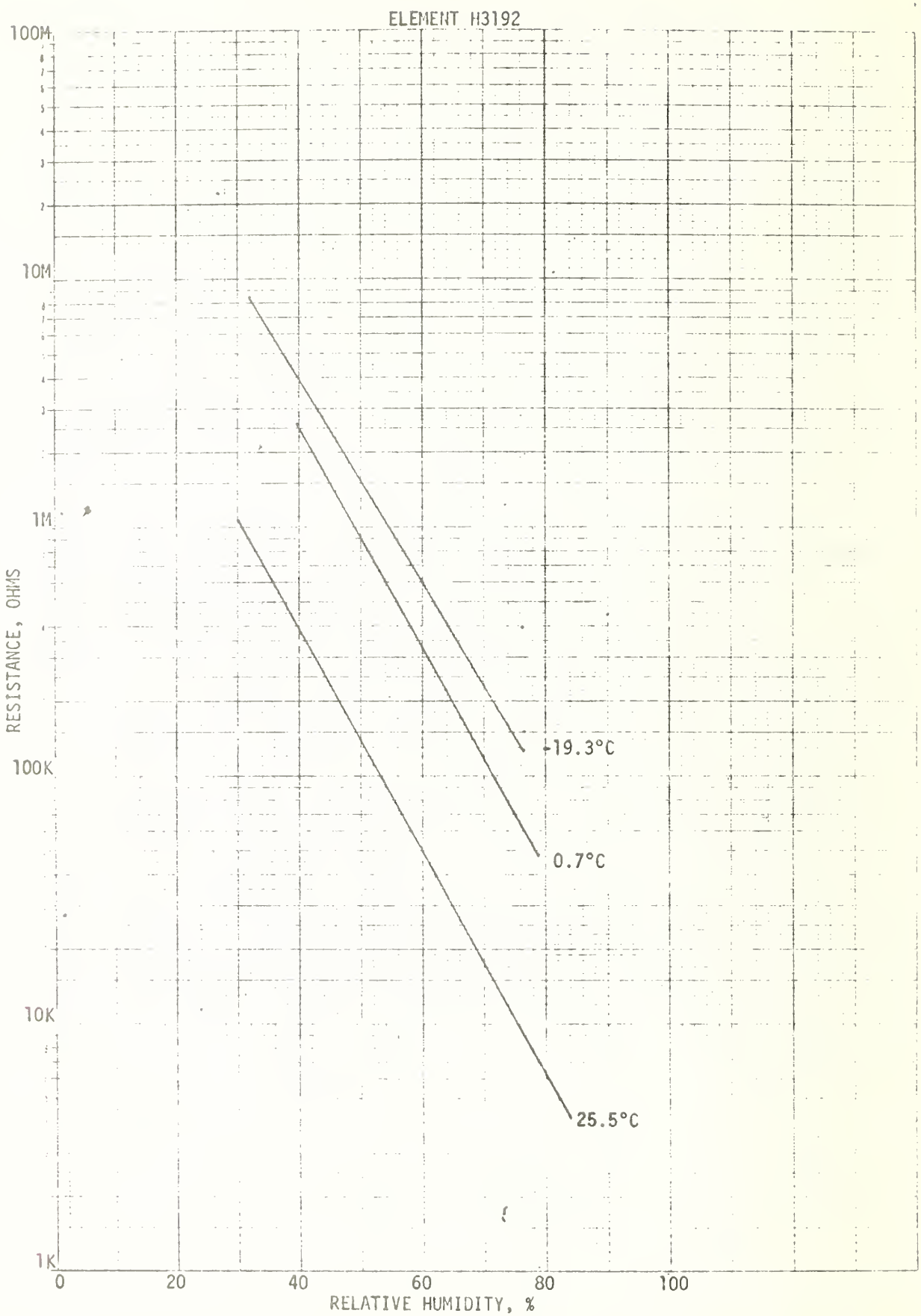

FIGURE 4. Calibration at several temperatures, element H3192.

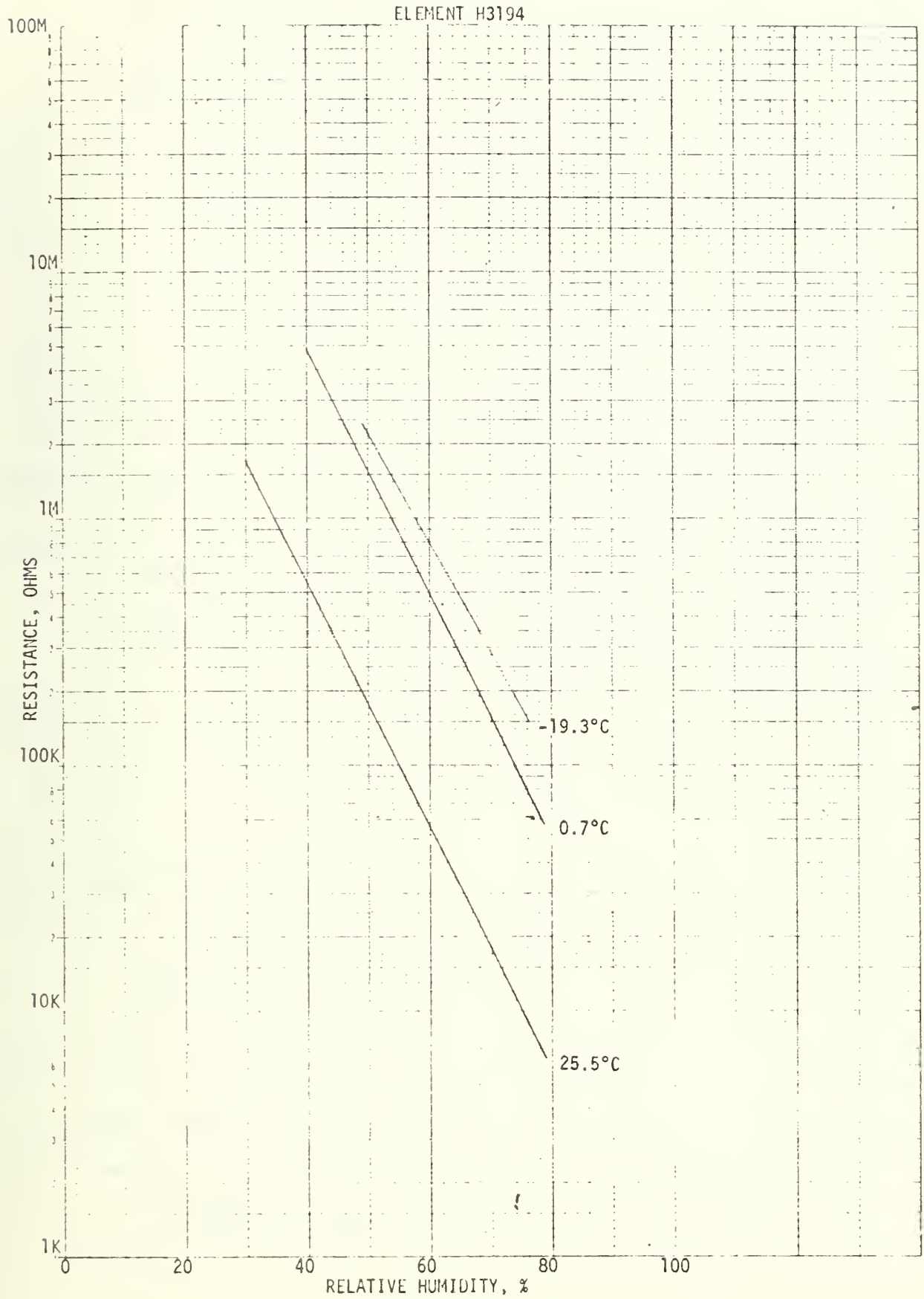

FIGURE 5. Calibration at several temperatures, element H3194.

The treatment in reference 9 is briefly outlined here in the interest of completeness. Calibration data from reference 2 for elements calibrated at nominal temperatures of 40°, 20°, 0°, -20° and -40°C are treated. The data were fitted in the nominal region $\frac{p}{p_s}$ = 0.25 to 0.85 by an equation of the form

$$\log \quad R = a + b \frac{p}{p_s} \quad . \qquad (30)$$

It was determined that the values of b for the five temperatures were not statistically significantly different, consequently, the value of b for 0°C was assigned as the slope for each of the calibration temperatures and the values of the intercept were adjusted to correspond to this value of the slope. Assigning the same slope for each of the curves permits the assignment of the temperature dependence of $\log_{10} R$ to adjusted intercepts, thus

$$\log \quad R \left(\frac{p}{p_s}, T \right) = a' \ (T) + b' \ \frac{p}{p_s} \ ,$$

where a' is the intercept adjusted to correspond to the assigned slope b'. For each temperature, a straight line of slope b' was drawn through the point at $\frac{p}{p_s}$ = 0.50. The intercepts of each of these straight lines is a' for the particular temperature. The plot of a' against temperature is shown in figure 6. A functional relationship between a' and T derived from curve-fitting the data of figure 6 would permit automatic data processing of element resistance data to arrive at indicated RH for any temperature in the range 40° to -40°C.

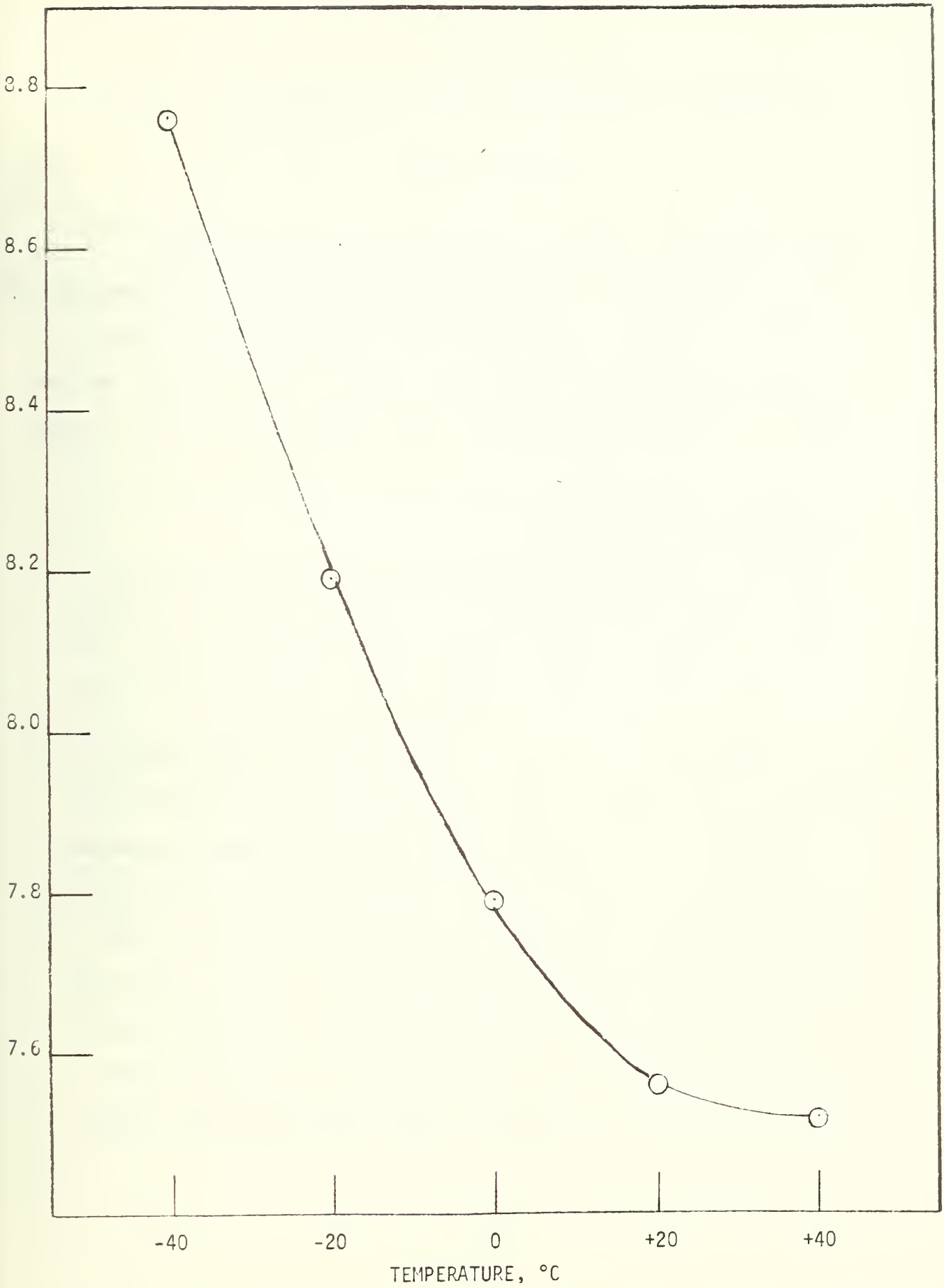

FIGURE 6. Plot of adjusted intercept, a', of equation 29 against temperature.

4. DISCUSSION

The values of the parameters a and b in the equation

$$\ln R = a + b \frac{p}{p_s} \qquad (1)$$

relating element resistance, R, to the relative pressure of water vapor, $\frac{p}{p_s}$, for the elements calibrated at room temperature on September 6, 1975 are tabulated in table 3. The values of the parameters for subsequent calibrations are tabulated in tables A-10 through A-13. For comparison, the parameters for element K2 of reference 9 for region II ($\frac{p}{p_s}$ = 0.335 to 0.805) are included in the tables. In the present work, equation 1 applies to the range $\frac{p}{p_s}$ = 0.29 to 0.845.

Application of the "t test" [11] indicates that the values of b for elements from suppliers A and B in the tables are not statistically significantly different, at the 1 percent level, from the value of b for element K2 of reference 9. The values of b for 3 elements (A3-D, A4-D and C2-D) from supplier D are statistically significantly different, at the 1 percent level, from the value of b for element K2 of reference 9. Since the functional dependence of element resistance on relative pressure of water vapor is reflected in the value of b, it can be concluded that in respect to room temperature calibration the elements produced by suppliers A and B are typical of those produced at NBS. The elements supplied by suppliers D and E, although the values of b depart significantly from that for element K2 of reference 9 and from those for elements from suppliers A and B, are nevertheless useful.

Table 3. Room Temperature Calibration Parameters, a and b, for Elements Calibrated on September 6, 1975. ($\ln R = a + b \frac{p}{p_s}$).

Element-Supplier	b	a
A1 - B	-8.21568	15.31044
A2 - B	-8.30881	15.75718
C3 - B	-8.11827	15.92886
C4 - B	-7.73982	15.85565
III1 - A	-8.01530	14.85332
III2 - A	-7.69423	14.89861
III3 - A	-7.76116	15.14089
III4 - A	-7.92297	15.32379
mean for supplier B	-8.09565	15.71303
mean for supplier A	-7.84842	15.05415
(1) mean for 8 elements	-7.97203	15.38359
estimate of standard deviation for 8 elements	0.23115	
estimate of standard deviation of the mean for 8 elements	0.08172	
(2) element K2 of reference 9	-8.12993	16.03712
$\frac{(1)}{(2)}$	0.98058	0.95925

The value of a, the intercept, in equation 1 is influenced by the quality of the electrode patterns on the substrates and therefore is not considered in detail here. It is desirable, however, that the value of a be reasonably small since ultimately the problem of measuring very high resistances is accentuated by this parameter.

The low temperature calibration data, although leaving much to be desired due to the inadequacy of the circuitry used, give qualitative encouragement that the low temperature performance of some of the elements might be typical of that of elements produced at NBS.

The calibration equations derived above provide analytical expressions relating element resistance (or conductance) to relative humidity (or relative vapor pressure of water). The effectiveness of the analysis is indicated by the agreement between calculated and "measured" conductance (columns (4) and (5) in table 2) as expressed by the ratio of these [($\frac{(4)}{(5)}$ in table 2)]. The ratio is seen to range from 0.948 to 1.103 (94.8 to 110.3%). The uncertainty in the measurement of resistance is estimated to be about ± 5% over most of the range of resistance. The uncertainty in resistance due to the uncertainty in the values of the RH points established by the saturated salt solutions (estimated to be ± 0.5% RH) is estimated to be ± 4%. The uncertainty in the resistance measurement is considered to be random, the uncertainty in the values of the RH points is considered to be systematic. Combining the two uncertainties in resistance by addition, results in an uncertainty of ± 9%. On this basis the agreement between the calculated and "measured" values of conductance, approximately -5 to +10%, is seen to be quite satisfactory.

4.1 Physical Adsorption and Humidity Element Functioning

Empirical equations of the form of equation 23,

$$G' = a + b \ln \frac{p}{p_s} + c \left(\frac{p}{p_s}\right)^d + f\left(\frac{p}{p_s}\right)^h \qquad (30)$$

represent the relationship between element conductance, G, and relative vapor pressure of water, $\frac{p}{p_s} = \frac{RH}{100}$, and can be used to generate calibration curves or equations, i.e., element resistance versus relative humidity. These equations also provide insight into the physical processes involved in the functioning of the element.

It has been hypothesized that the element functions by the physical adsorption of water vapor on the barium fluoride film, the amount of adsorbed water vapor depending on the relative pressure of water vapor. The adsorbed water vapor increases the surface conductance of the film. A plot of conductance versus relative pressure of water vapor should therefore represent an adsorption isotherm.

Many theoretical isotherm equations exist and attempts have been made by others to apply them to physical adsorption data with varying degrees of success. These include the isotherm equations of Langmuir, BET (Brunauer, Emmett and Teller), Fruendlich, Harkins-Jura, Henry, Frenkel-Halsey-Hill and many others. The approach taken in the present work has been to decompose the "S-shaped" plot of conductance, G, versus relative pressure of water vapor, $\frac{p}{p_s}$, into its three constituent parts, fit empirical equations to the parts and combine these empirical equations. Following this empirical treatment of the data, we then inquire which, if any, of the theoretical isotherm equations are represented by the empirical equations.

It has been shown above that a plot of conductance versus $\frac{p}{p_s}$ is a composite of three separate curves. The existence of the three separate curves has been attributed to three distinct modes of physical adsorption. It is tempting to describe these modes as the conventional unimolecular and multimolecular adsorption and capillary condensation. It is also possible to hypothesize the existence of three classes of adsorption sites. We shall here adhere to referring to distinct modes of adsorption.

A plot of conductance against $\frac{p}{p_s}$ has the shape of the Type II isotherm in the Brunauer designation [12]. A plot of the first two terms of equation 30 has the shape of the Type I isotherm, a plot of the third term and a plot of the fourth term have the shape of the Type III isotherm. Therefore, the conductance - $\frac{p}{p_s}$ isotherm (in itself a Type II isotherm) is a composite of a Type I isotherm and two Type III isotherms. This is an <u>important</u> result of more general application.

The first two terms of equation 30, a + b ln $\frac{p}{p_s}$, are an empirical fit of the data in the 12 to 22.5% RH region with parameters adjusted by iteration to apply to the entire range of RH. The third and fourth terms expressed as conductances are

$$G_2' = c\left(\frac{p}{p_s}\right)^d , \tag{31}$$

$$G_3' = f\left(\frac{p}{p_s}\right)^h . \tag{32}$$

Equations 31 and 32 are of the form of the Freundlich equation [12]

$$v = kp^n , \tag{33}$$

where v is the volume of gas adsorbed and p is the equilibrium pressure. Therefore, the analysis of the data has produced an empirical equation for the Type I isotherm, equations of the form of the Freundlich equation for two Type III isotherms and a decomposition of a Type II isotherm into a Type I isotherm and two Type III isotherms.

5. CONCLUSIONS

Commercial sources for barium fluoride film electric hygrometer elements have been developed. Elements produced by at least two of these sources appear to be typical of those produced at NBS. This represents the successful transfer of technology from the developer of the element in the Federal Government to the private sector and should insure the availability of the element for general use. This general use includes missile climatology and routine radiosonde use.

Calibration equations for the elements have been developed and insight into the physical processes involved in the functioning of the element has been gained by analysis of calibration data. It has been shown that the conductance - $\frac{p}{p_s}$ isotherm (in itself a Type II isotherm in the Brunauer designation of physical adsorption isotherms) is a composite of a Type I isotherm and two Type III isotherms. The two Type III isotherm equations are of the form of the Freundlich theoretical isotherm equation. These results represent the solution of a long-standing problem in adsorption and have general application to other adsorption systems in addition to the water vapor-barium fluoride film system.

It is estimated that in the intermediate RH region, 33.5 percent to 80.5 percent, measurements of RH using the commercially produced elements would be uncertain by about 5 percent RH. There is not sufficient data to make estimates of the uncertainties in the other regions.

6. REFERENCES

[1]. F. E. Jones, "Hygrometer Elements," U. S. Patent 3,058,079 (1962).

[2]. F. E. Jones and A. Wexler, "A Barium Fluoride Film Hygrometer Element," J. Geophys. Res. 65, 2087 (1960).

[3]. F. E. Jones, "Performance of the Barium Fluoride Film Hygrometer Element on Radiosonde Flights," J. Geophys. Res. 68, 2735 (1963).

[4]. F. E. Jones, "Study of the Storage Stability of the Barium Fluoride Film Electric Hygrometer Element," J. Res. NBS 71C, 199 (1967).

[5]. B. R. Bean and R. O. Gilmer, "Comparison of Barium Fluoride Humidity Element with the Microwave Refractometer for Studies of Rapid Fluctuations of Atmospheric Humidity," Radio Science 4, 1155 (1969).

[6]. B. R. Bean and Q. L. Florey, "A Field Study of the Effectiveness of Fatty Alcohol Mixtures as Evaporation Reducing Monomolecular Films," Water Resources Research 4, 206 (1968).

[7]. S. M. Goltz, C. B. Tanner, G. W. Thurtell and F. E. Jones,"Evaporation Measurements by an Eddy Correlation Method," Water Resources Research 6, 440 (1970).

[8]. H. K. Weickmann, A. R. Tebo and F. E. Jones, "Temperature and Humidity Conditions in Cumulus Mediocris," Conference on Cloud Physics, Fort Collins, Colorado, August 24-27, 1970, pp. 177, 178.

[9]. F. E. Jones, "Barium Fluoride Film Humidity Element Calibration Analysis, Applications and other Developments", NBS Report 10058, July, 1969.

[10]. A. Wexler and R. D. Daniels, Jr., "Pressure-Humidity Apparatus," J. Res. NBS 48, 269 (1952).

[11]. W. J. Youden, Statistical Methods for Chemists (John Wiley & Sons, Inc., New York, 1951), pp. 47-49.

[12]. S. Brunauer, The Adsorption of Gases and Vapors, Vol. I, Physical Adsorption (Princeton University Press, Princeton, New Jersey, 1943), p. 150.

7. FIGURE CAPTIONS

8. LIST OF TABLES

9. APPENDIX A

ADDITIONAL FIGURES AND TABLES

Figures and tables which have not been interleaved with the text are presented on the following pages of this appendix.

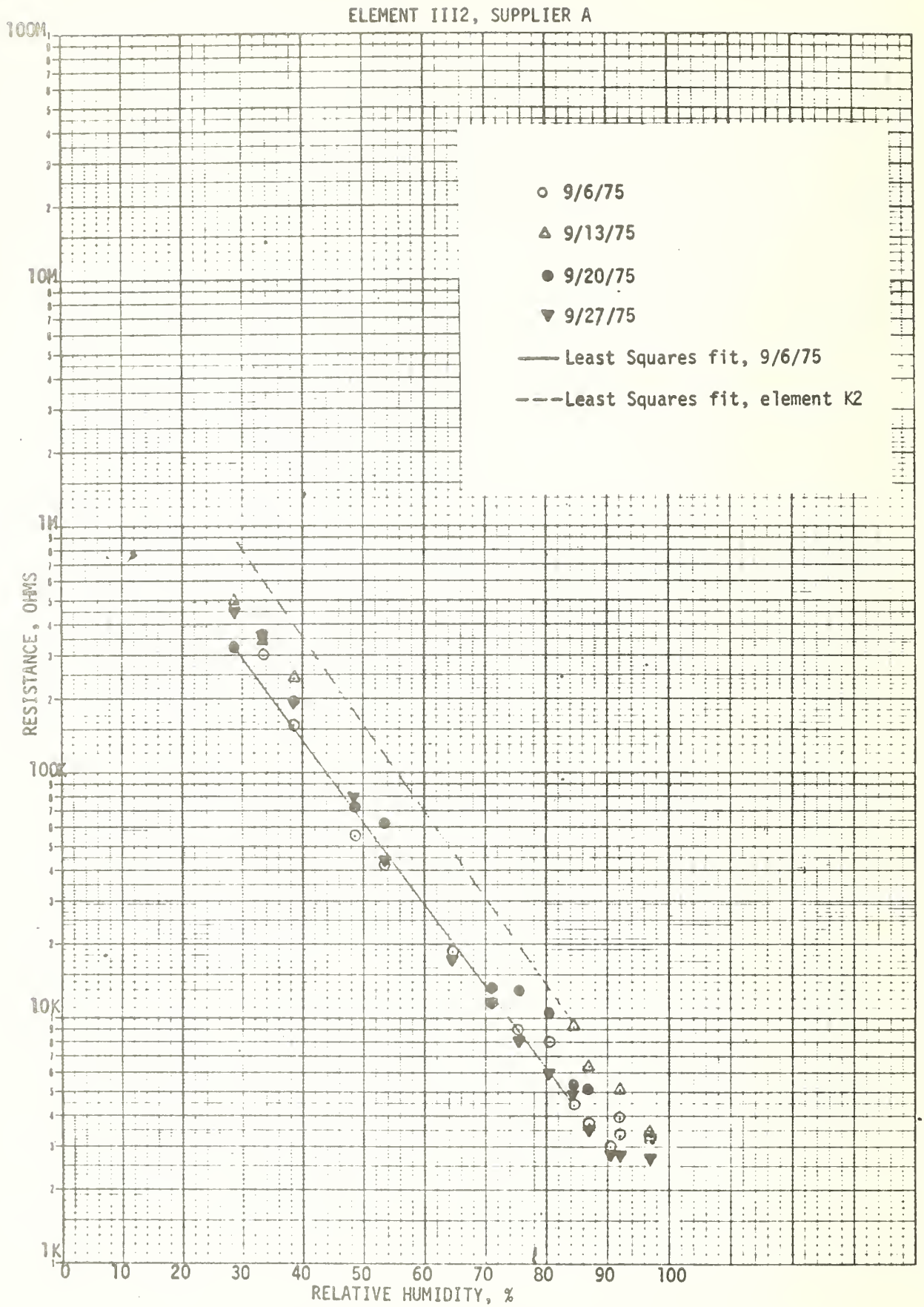

FIGURE A-1. Room temperature calibration, element III2, supplier A.

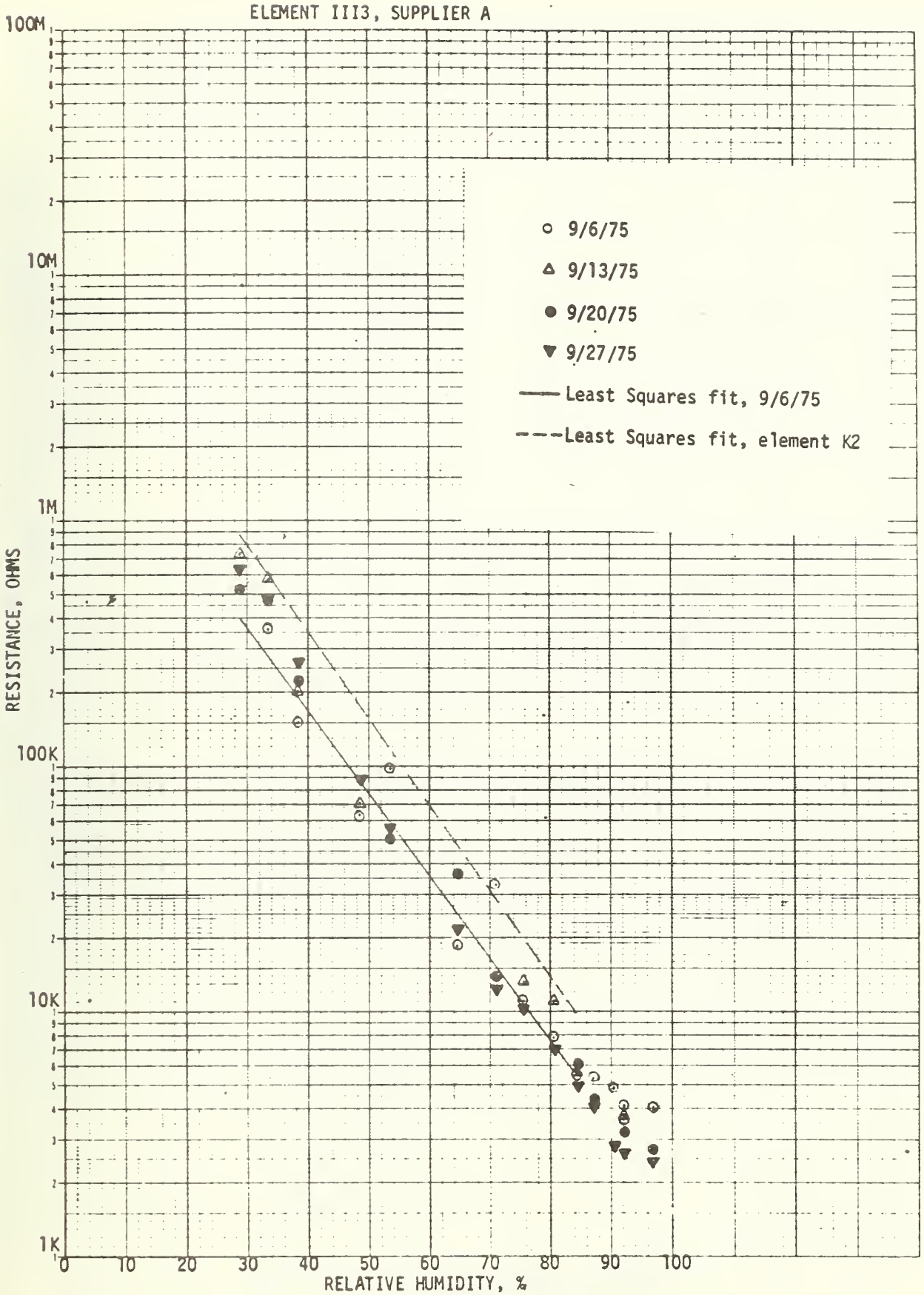

FIGURE A-2. Room temperature calibration, element III3, supplier A.

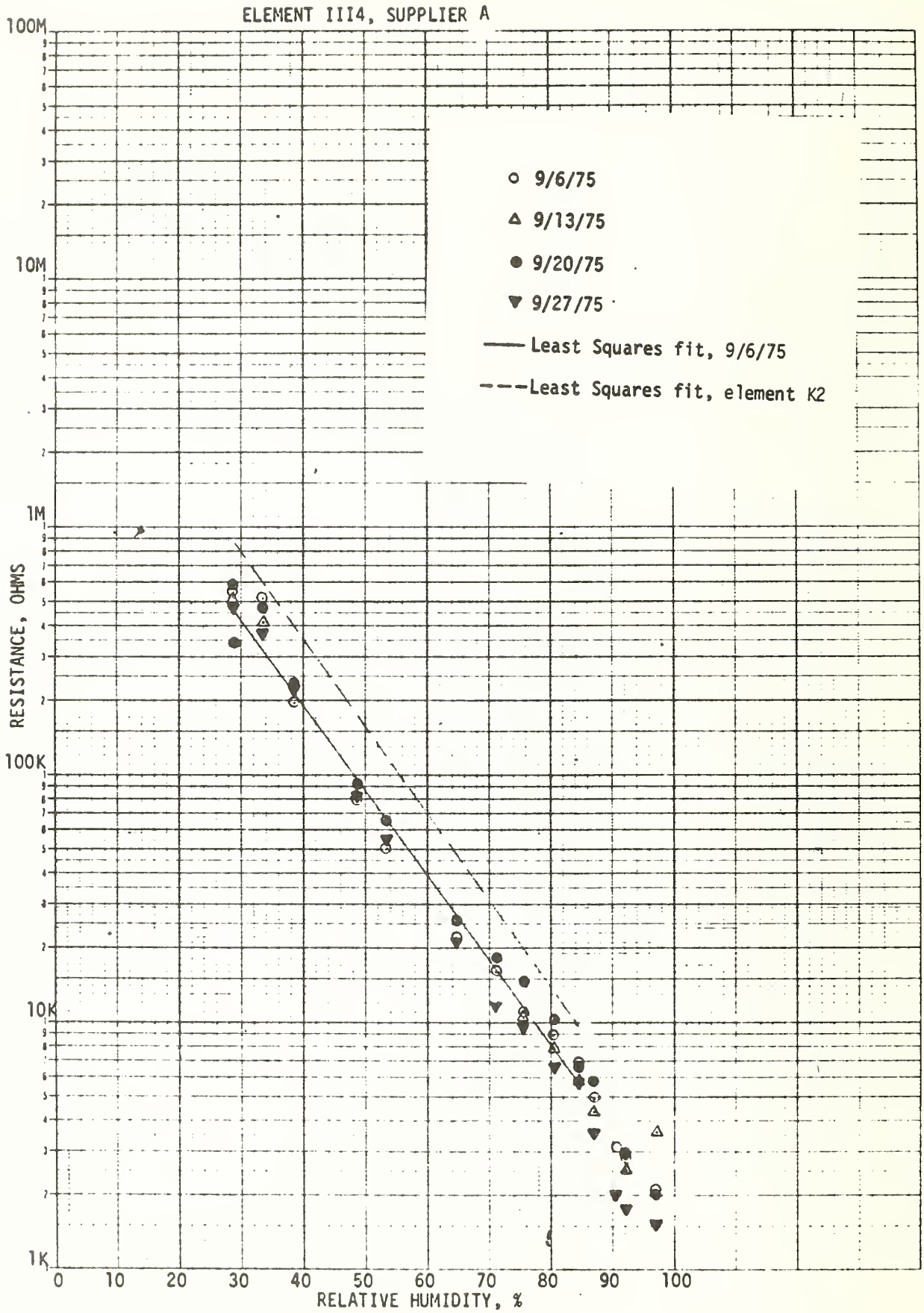

FIGURE A-3. Room temperature calibration, element III4, supplier A.

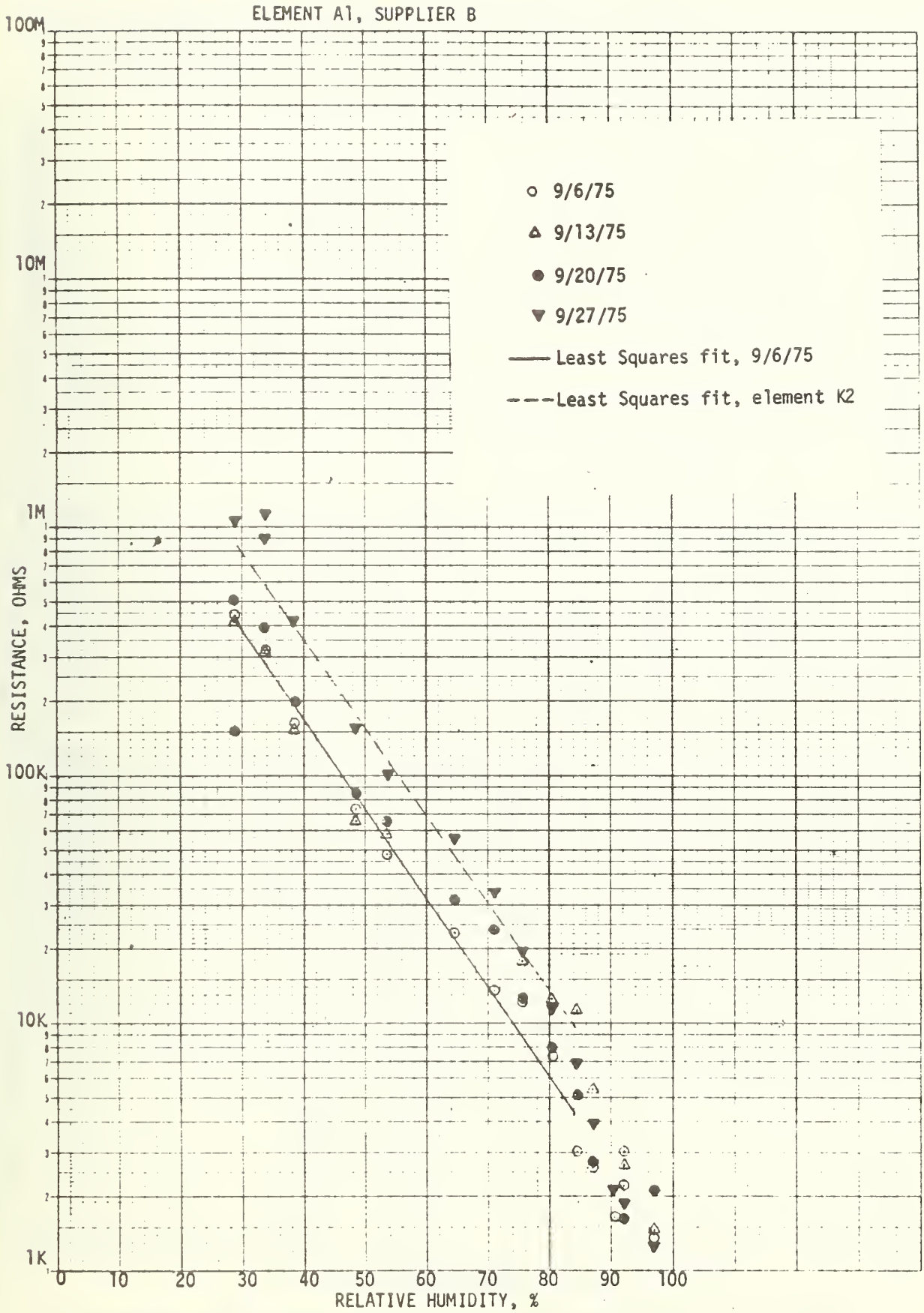

FIGURE A-4. Room temperature calibration, element A1, supplier B.

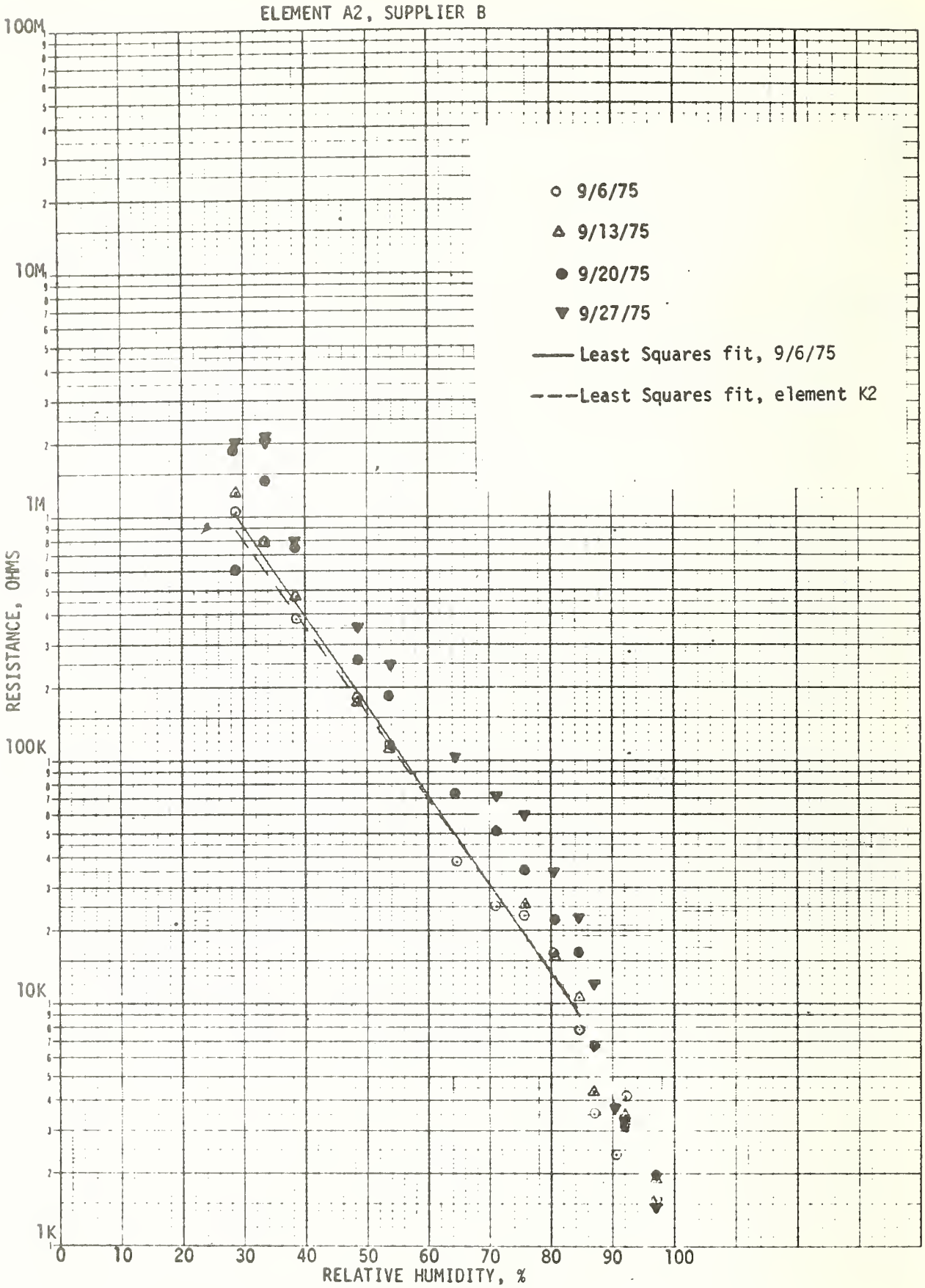

FIGURE A-5. Room temperature calibration, element A2, supplier B.

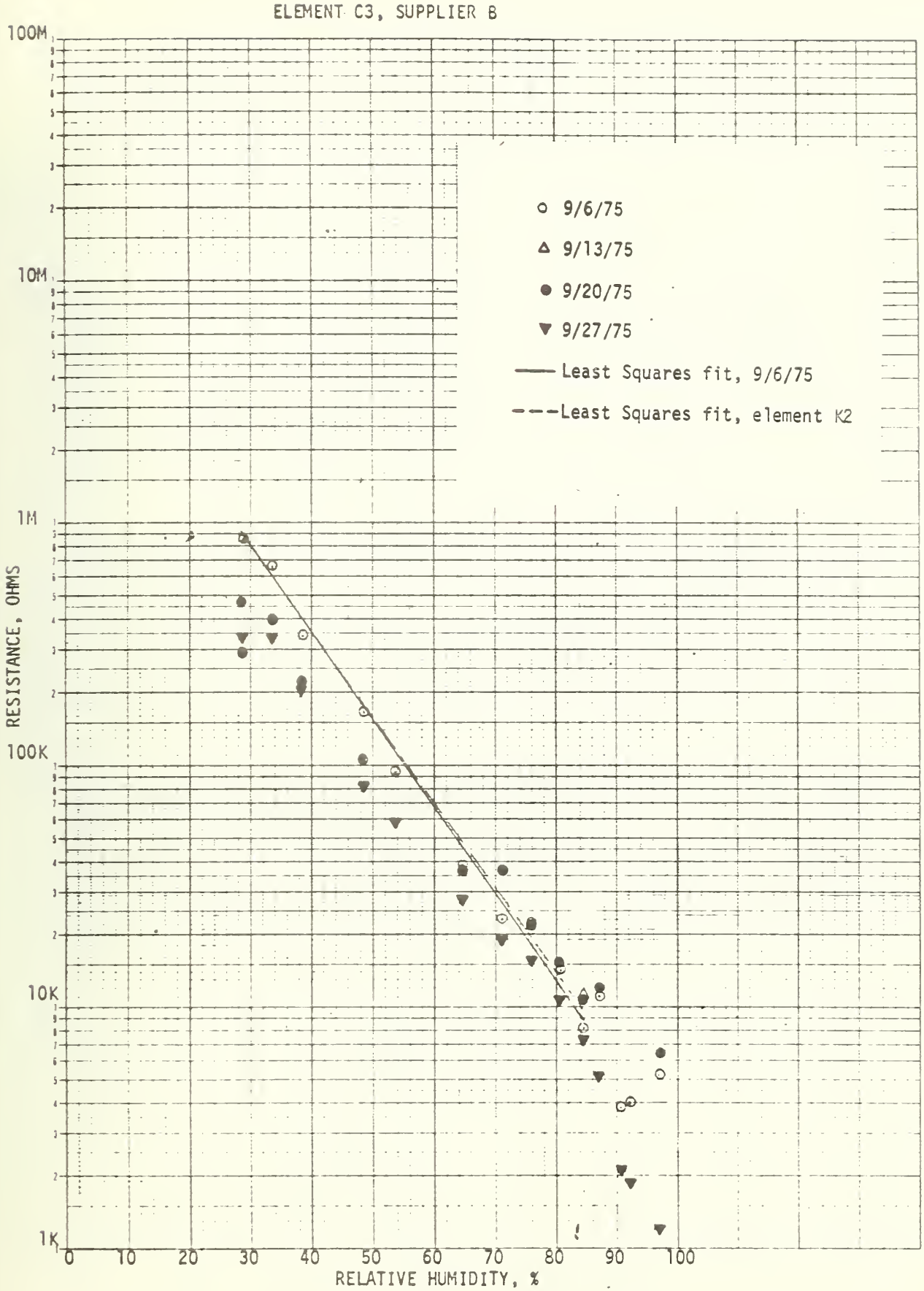

FIGURE A-6. Room temperature calibration, element C3, supplier B.

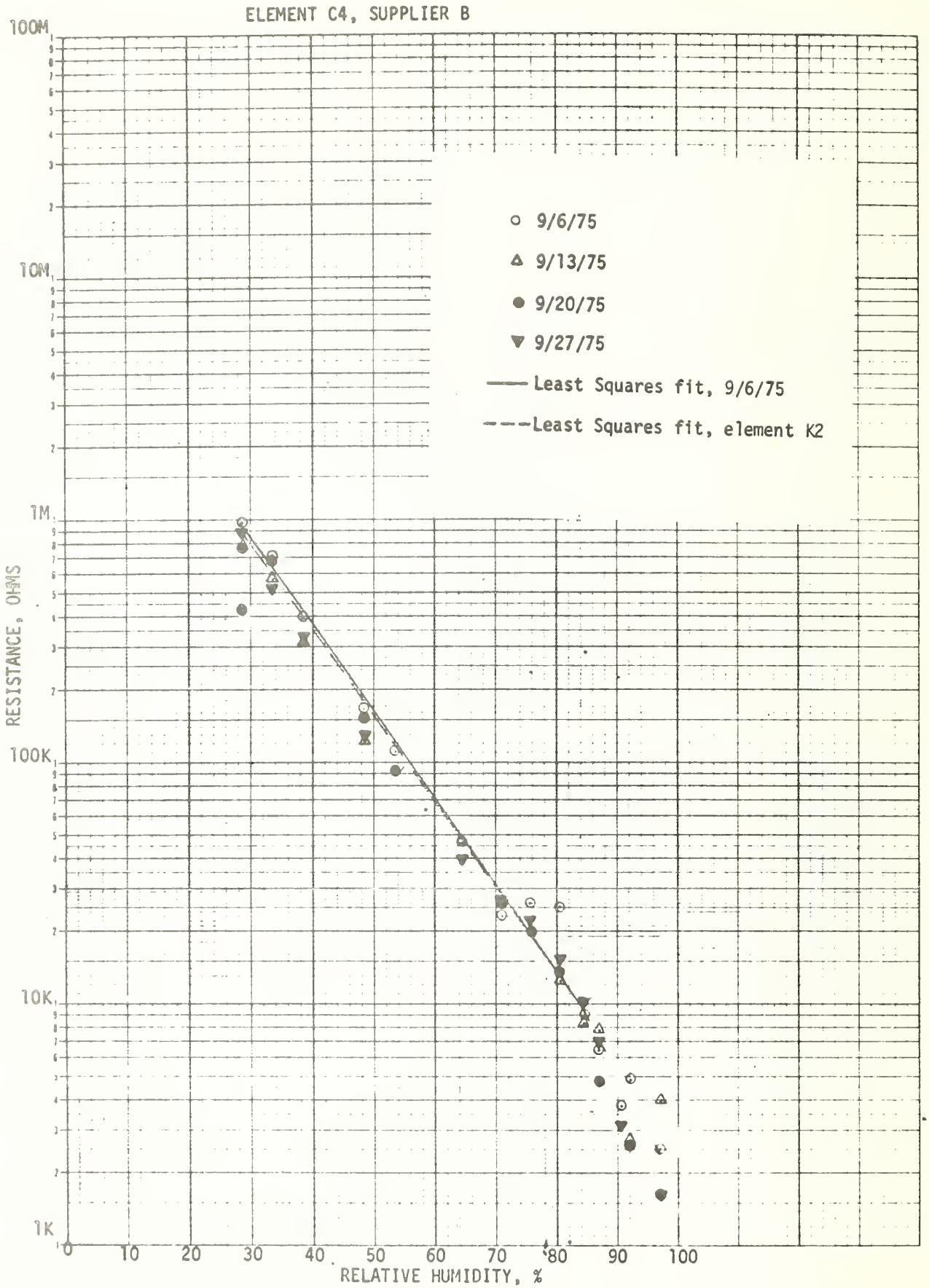

FIGURE A-7. Room temperature calibration, element C4, supplier B.

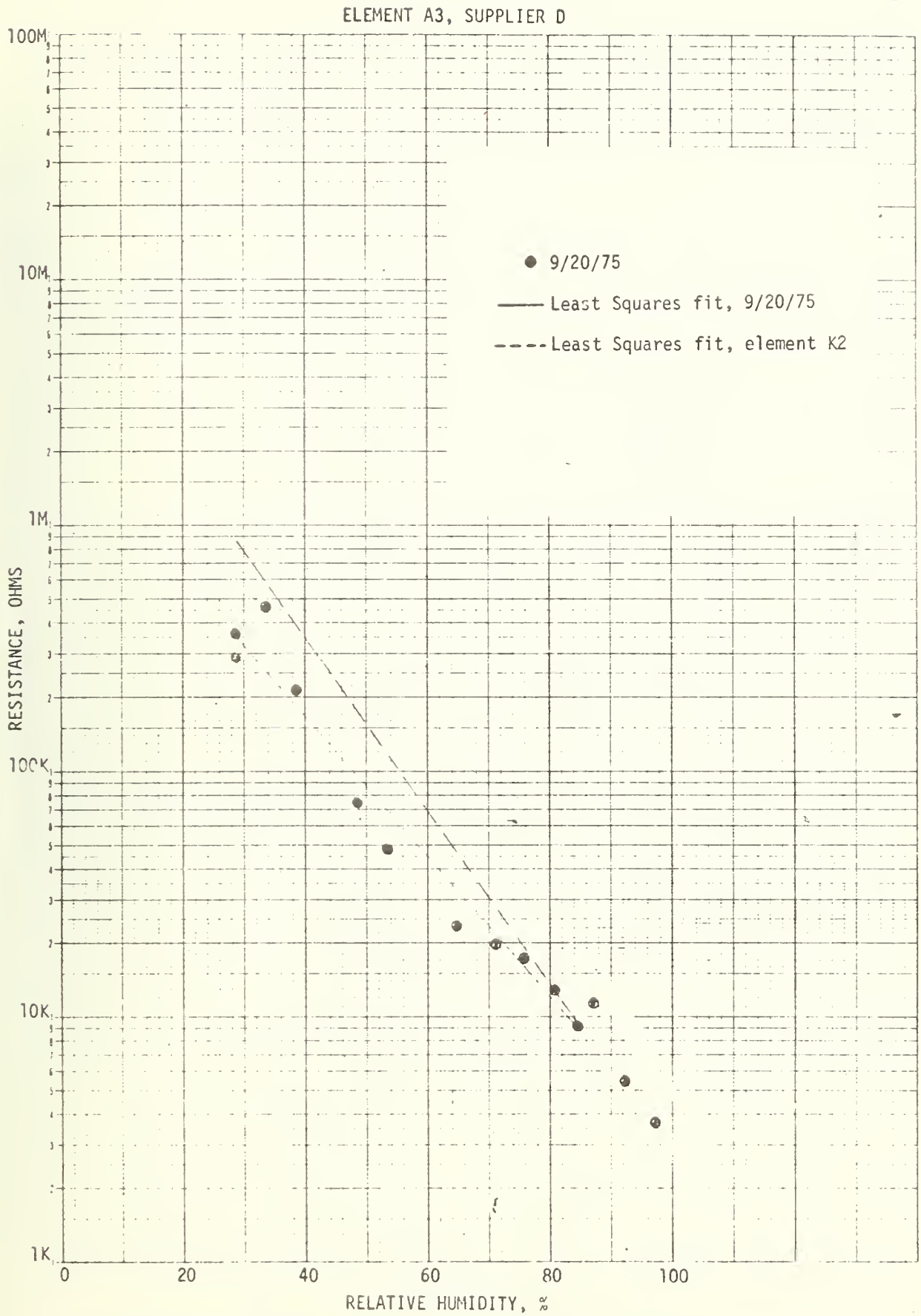

FIGURE A-8. Room temperature calibration, element A3, supplier D.

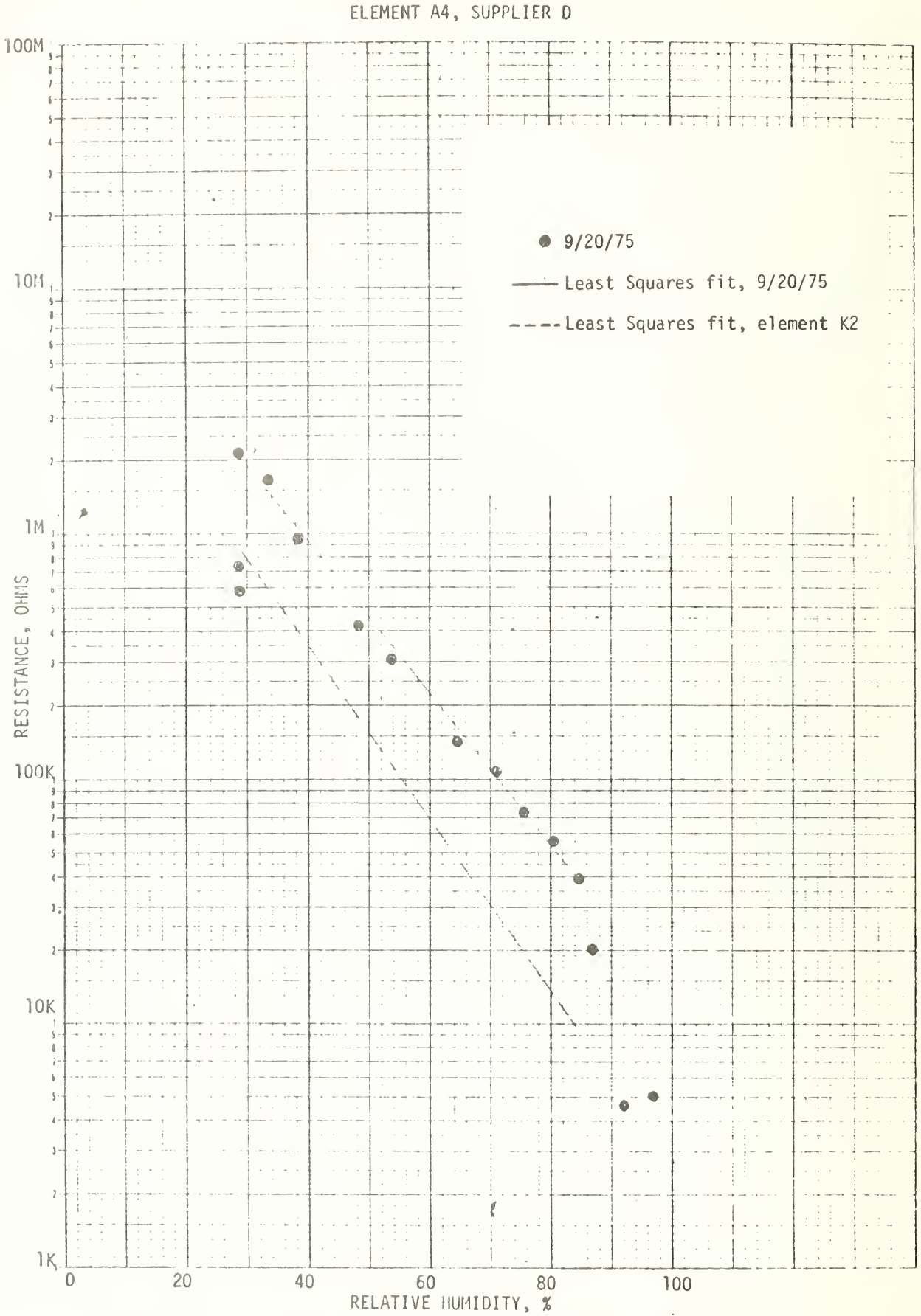

FIGURE A-9. Room temperature calibration, element A4, supplier D.

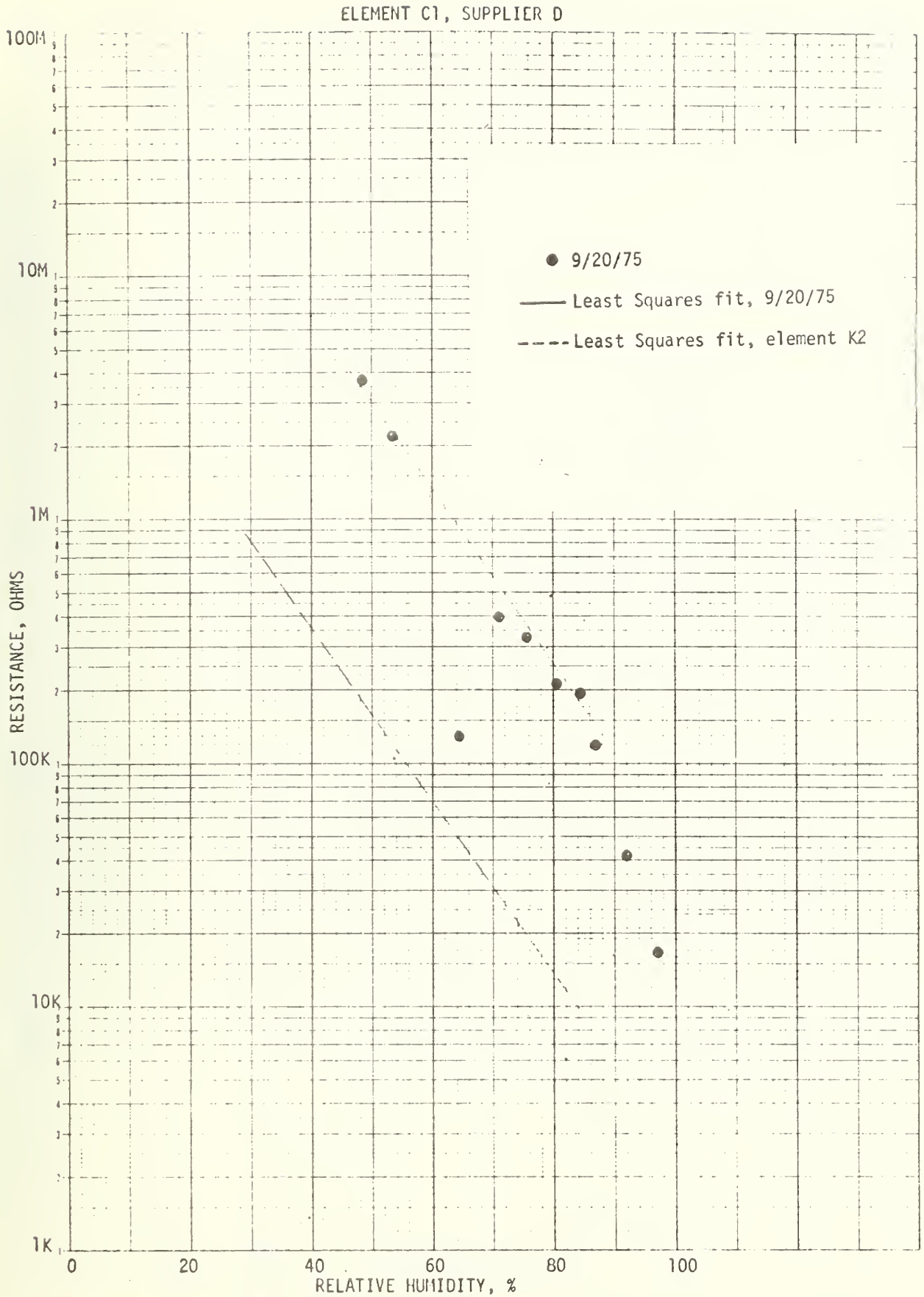

FIGURE A-10. Room temperature calibration, element C1, supplier D.

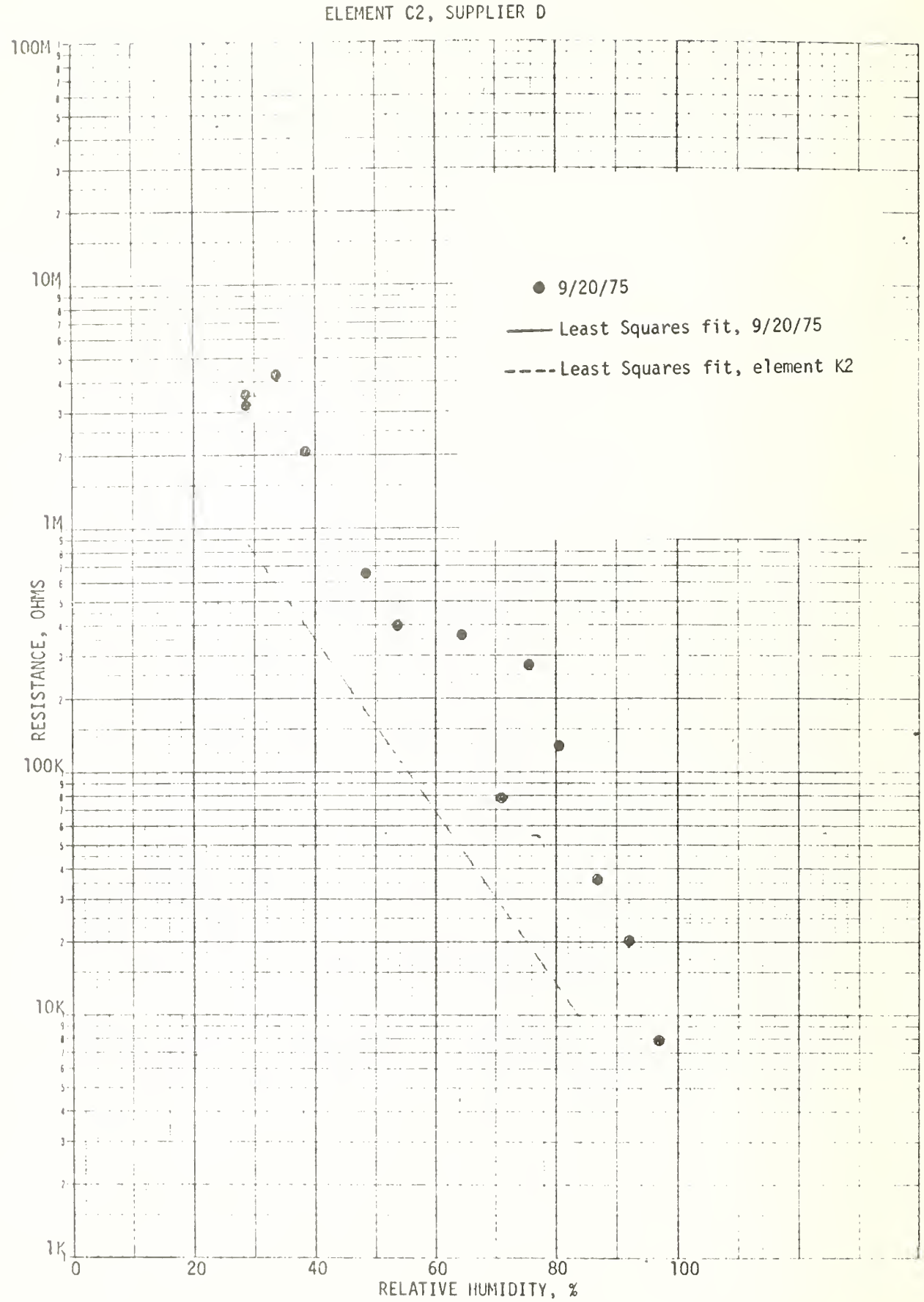

FIGURE A-11. Room temperature calibration, element C2, supplier D.

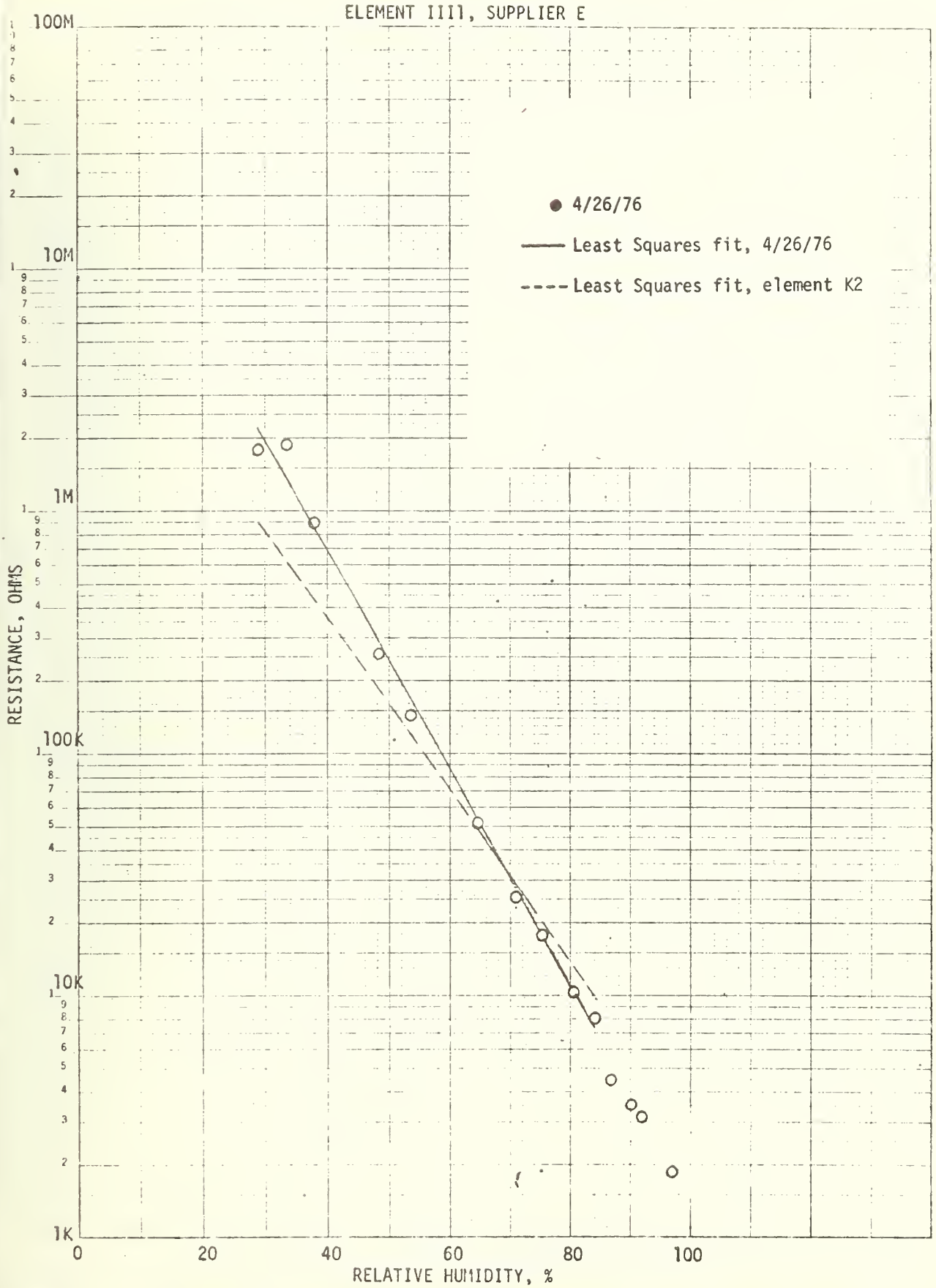

FIGURE A-12. Room temperature calibration, element IIII, supplier E.

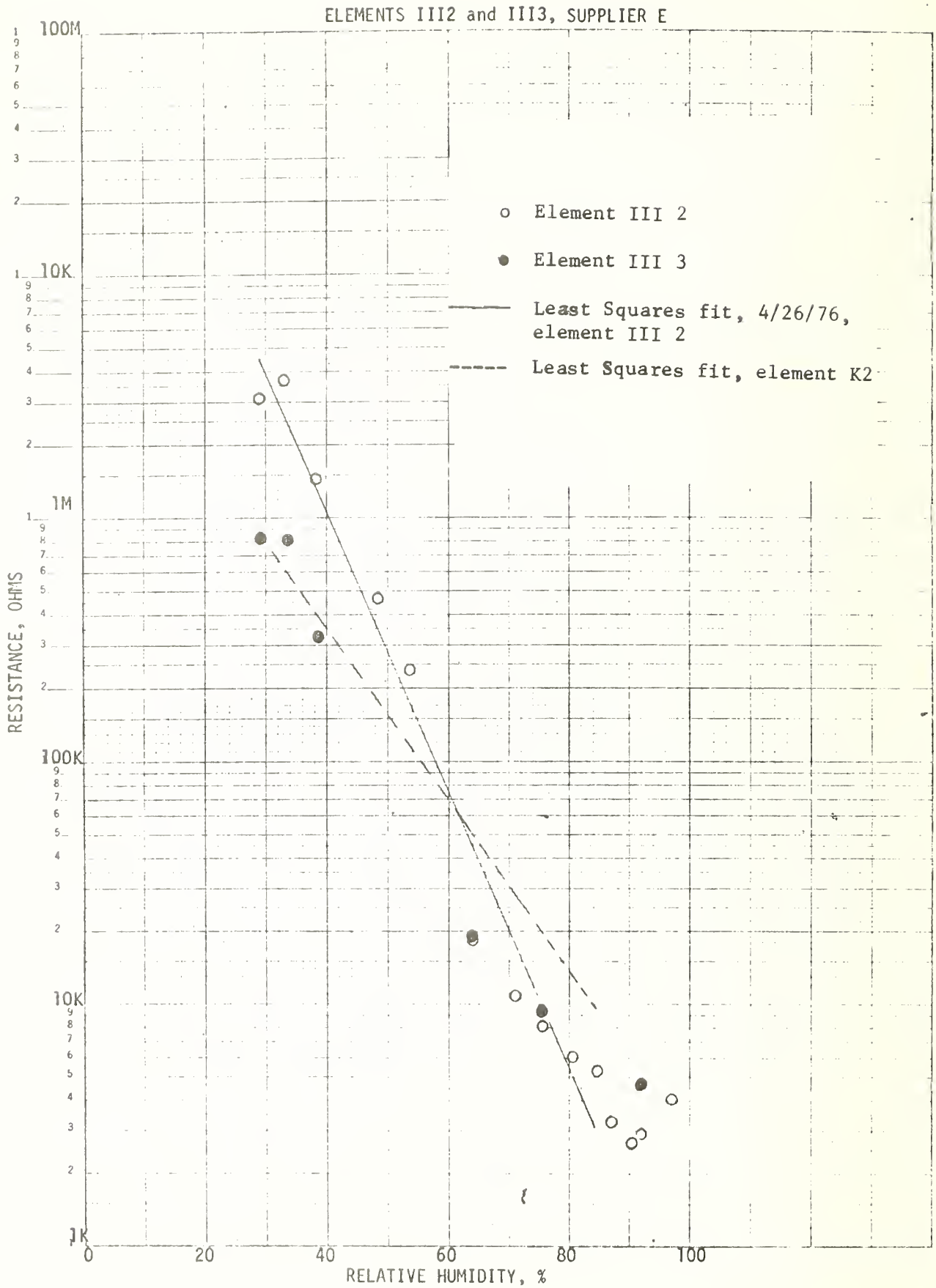

FIGURE A-13. Room temperature calibration, elements III2 and III3, supplier E.

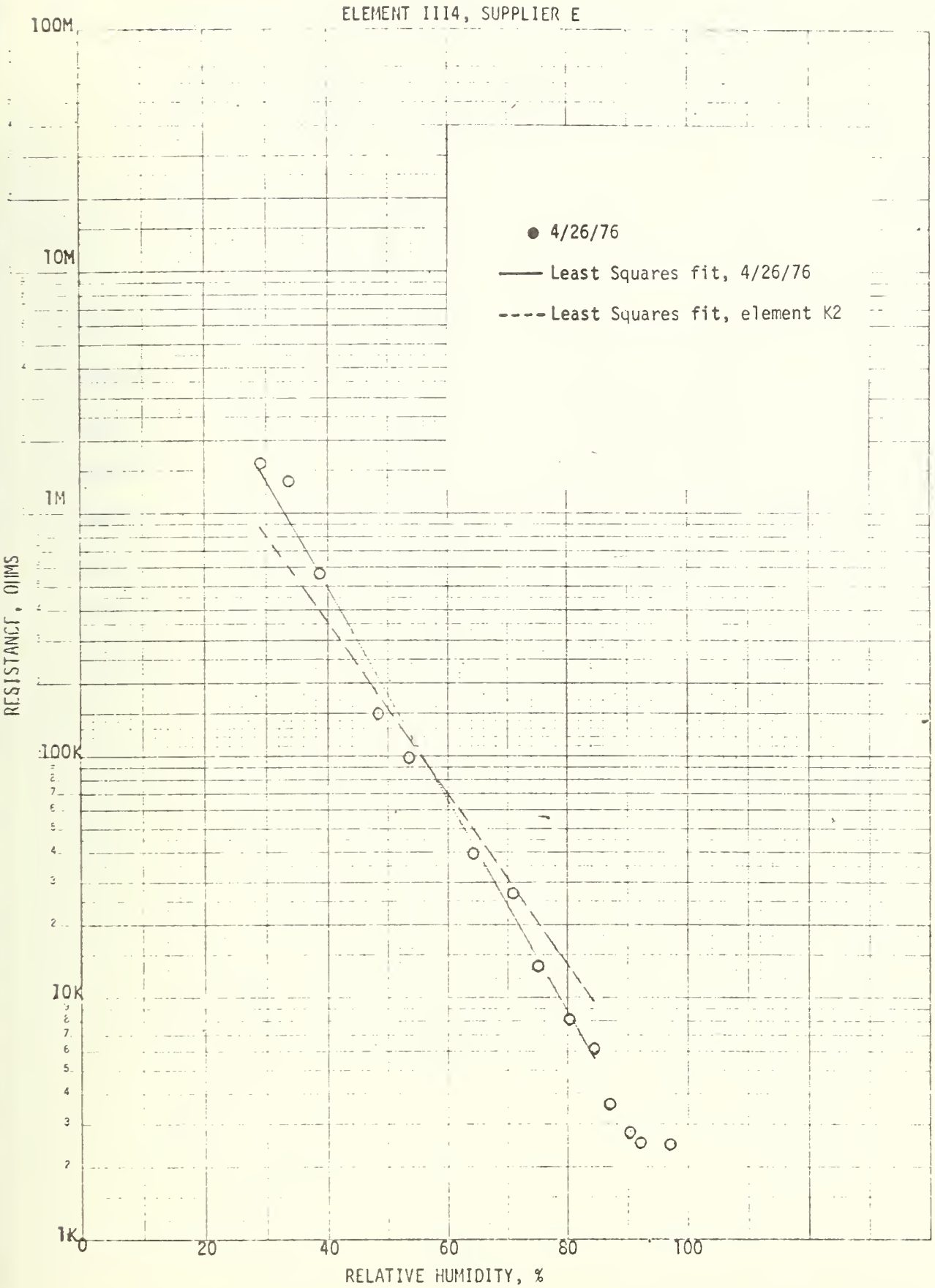

FIGURE A-14. Room temperature calibration, element III4, supplier E.

Table A-1. Values of Conductance in Region II, G_{II}, and Relative Pressure of Water Vapor, $\frac{p}{p_s}$, Calculated Using Equations 3 and 4.

(1) G_{II}, in micromohos	(2) $\frac{p}{p_s}$	(3) Calc. G_{II}, in micromhos	(4) calc. $\frac{p}{p_s}$	$\frac{(3)}{(1)}$	(4) - (2)
1.61	0.335	1.71	0.327	1.062	-0.008
2.56	0.385	2.55	0.385	0.996	0.000
5.35	0.485	5.68	0.477	1.062	-0.008
8.70	0.535	8.48	0.538	0.975	+0.003
21.1	0.645	20.47	0.649	0.970	+0.004
36.4	0.710	34.45	0.717	0.946	+0.007
48.8	0.755	49.40	0.753	1.012	-0.002
75.2	0.805	73.72	0.807	0.980	+0.002

Table A-2. Values of Conductance in Region III, G_{III}, and Relative Pressure of Water Vapor, $\frac{p}{p_s}$, Calculated Using Equations 5 and 6.

(1) G_{III}, in micromhos	(2) $\frac{p}{p_s}$	(3) Calc. G_{III}, in micromhos	(4) calc. $\frac{p}{p_s}$	$\frac{(4)}{(3)}$	(4) - (2)
108	0.845	108.7	0.845	1.006	0.000
152	0.870	149.2	0.871	0.982	+0.001
270	0.920	281.1	0.917	1.041	-0.003
465	0.955	438.0	0.960	0.942	+0.005
513	0.970	529.8	0.967	1.033	-0.003

Table A-3. Values of G_3, the Difference Between the Values of the Conductance in Regions II and III, Calculated Using Equations 3 and 5.

(1) calc. G_{III}, in micromhos	(2) calc. G_{II}, in micromhos	$G_3 \equiv (1) - (2)$, in micromhos	$\frac{p}{p_s}$
108.7	101.6	7.1	0.845
149.2	124.1	25.1	0.870
281.1	185.2	95.9	0.920
438.0	245.0	193.0	0.955
529.8	276.3	253.5	0.970

Table A-4. Values of G_3, the Difference Between the Calculated Values of the Conductance in Regions II and III, and $\frac{p}{p_s}$, Calculated Using Equations 10 and 11.

(1) G_3, in micromhos	(2) $\frac{p}{p_s}$	(3) calc. G_3, in micromhos	(4) calc. $\frac{p}{p_s}$	$\frac{(3)}{(1)}$	(4) - (2)
7.1	0.845	9.36	0.836	1.318	-0.009
25.1	0.870	19.41	0.879	0.773	+0.009
95.9	0.920	78.42	0.927	0.818	+0.007
193.0	0.955	199.4	0.954	1.033	-0.001
253.5	0.970	294.3	0.964	1.161	-0.006

Table A-5. Value of G_I, the Calculated Value of the Conductance in Region I, and $\frac{p}{p_s}$, Calculated Using Equations 14 and 13.

(1) G_I, in micromhos	(2) $\frac{p}{p_s}$	(3) calc. G_I, in micromhos	(4) calc. $\frac{p}{p_s}$	$\frac{(3)}{(1)}$	(4) - (2)
0.500	0.120	0.500	0.120	1.000	0.000
0.714	0.175	0.713	0.175	0.999	0.000
0.855	0.225	0.855	0.225	1.000	0.000

Table A-6. Values of G_2, the Conductance Due to Adsorption Mode II, Calculated Using Equations 3, 14 and 16.

	(1) calc. G_{II}, in micromhos	(2) calc. G_I, in micromhos	(3) $G_2 \equiv$ (1)-(2), in micromhos	(4) calc. G_2, in micromhos	$\frac{(4)}{(3)}$	$\frac{p}{p_s}$
	0.306	0.500				0.120
Region I	0.475	0.713				0.175
	0.709	0.855				0.225
	1.710	1.080	0.630	0.626	0.994	0.335
	2.552	1.159	1.393	1.311	0.941	0.385
Region II	5.684	1.289	4.395	4.474	1.018	0.485
	8.464	1.345	7.119	7.537	1.059	0.535
	20.471	1.450	19.021	20.359	1.070	0.645
	34.450	1.505	32.945	33.413	1.029	0.710
	49.396	1.539	47.857	47.012	0.982	0.755
	73.720	1.576	72.144	66.101	0.916	0.805

Table A-7. Values of G_I and G_2, The Values of Conductance Due to Adsorption Modes I and II, Respectively, Calculated Using Equations 14 and 16, and the Sum of G_I and G_2.

	(1) G, in micromhos	(2) $\frac{p}{p_s}$	(3) calc. G_I, in micromhos	(4) calc. G_2, in micromhos	(5) (3) + (4) in micromhos	$\frac{(5)}{(2)}$
	0.500	0.120	0.500	0.003	0.503	1.006
↑ Region I	0.714	0.175	0.713	0.020	0.733	1.027
↓	0.855	0.225	0.855	0.076	0.931	1.089
↑	1.61	0.335	1.080	0.626	1.706	1.060
	2.56	0.385	1.159	1.311	2.470	0.965
Region II	5.35	0.485	1.289	4.474	5.763	1.077
↓	8.70	0.535	1.345	7.537	8.882	1.021
	21.1	0.645	1.450	20.359	21.809	1.034
	36.4	0.710	1.505	33.913	35.418	0.973
	48.8	0.755	1.539	47.012	48.551	0.995
	75.2	0.805	1.576	66.101	67.677	0.900

Table A-8. Values of G_1', and G_2', New Values of the Conductance Due to Adsorption Modes I and II, Respectively, Calculated Using Equations 17 and 18.

	(1) calc. G_1', in micromhos	(2) $\frac{p}{p_s}$	(3) calc. G_{II}', in micromhos	(4) $G_2' \equiv (?)-(1)$, in micromhos	(5) calc. G_2', in micromhos	(1)+(5), in micromhos
↑ Region I	0.504	0.120			0.004	0.508
	0.676	0.175			0.025	0.701
↓	0.790	0.225			0.091	0.881
↑	0.971	0.335	1.710	0.739	0.706	1.677
	1.034	0.385	2.552	1.518	1.447	2.481
	1.139	0.485	5.684	4.545	4.762	5.901
Region II	1.184	0.535	8.464	7.280	7.898	9.082
↓	1.268	0.645	20.471	19.203	20.720	21.988
	1.312	0.710	34.450	33.138	34.000	35.312
	1.340	0.755	49.396	48.056	46.681	48.021
	1.369	0.805	73.720	72.351	64.980	66.349

Table A-9. Values of G_3', the New Value of Conductance Due to Adsorption Mode III, Calculated from the New Values of the Conductance Due to Adsorption Modes I and II, Calculated Using Equations 17 and 18, and the "Measured" Value of Conductance, G.

(1) calc. G_1', in micromhos	(2) $\frac{p}{p_s}$	(3) calc. G_2', in micromhos	(4) (1) + (3) in micromhos	(5) G, in micromhos	$G_3' = (5)-(4)$, in micromhos
1.391	0.845	83.448	84.84	108	23.2
1.404	0.870	96.990	98.39	152	53.6
1.430	0.920	129.391	130.82	270	134
1.447	0.955	156.871	158.32	465	307
1.454	0.970	170.002	171.46	513	342

Table A-10. Room Temperature Calibration Parameters, a and b, for Elements Calibrated on September 13, 1975. ($\ln R = a + b\,RH$).

	Element-Supplier	b	a
	A1 - B	-6.10005×10^{-2}	14.35188
	A2 - B	-8.09422×10^{-2}	16.13275
	C4 - B	-7.92993×10^{-2}	15.74331
	III1 - A	-7.77542×10^{-2}	14.95634
	III2 - A	-7.09167×10^{-2}	15.11538
	III3 - A	-7.94441×10^{-2}	15.45438
	III4 - A	-8.17878×10^{-2}	15.49869
	mean for A2-B and C4-B	-8.01208×10^{-2}	15.93803
	mean for supplier A	-7.74757×10^{-2}	15.25620
(1)	mean for 6 elements	-7.83574×10^{-2}	15.48348
	estimate of standard deviation for 6 elements	0.39050×10^{-2}	
	estimate of standard deviation of the mean for 6 elements	0.15942×10^{-2}	
(2)	element K2 of reference 9	-8.12993×10^{-2}	16.03712
	$\frac{(1)}{(2)}$	0.96381	0.96548

Table A-11.Room Temperature Calibration Parameters, a and b, for Elements Calibrated on September 20, 1975. ($\ln R = a + b\ RH$).

Element-Supplier	b	a
A1 - B	-7.82767×10^{-2}	15.31730
A2 - B	-8.40123×10^{-2}	16.73889
C3 - B	-6.72384×10^{-2}	14.93656
C4 - B	-8.13712×10^{-2}	15.96918
III1 - A	-8.19514×10^{-2}	15.05381
III2 - A	-7.67538×10^{-2}	15.15096
III3 - A	-8.22840×10^{-2}	15.57060
III4 - A	-7.73869×10^{-2}	15.35507
A3 - D	-7.01840×10^{-2}	14.90606
A4 - D	-7.02122×10^{-2}	16.48222
*C1 - D	$*-8.48717 \times 10^{-2}$	*19.13051
C2 - D	-7.15512×10^{-2}	17.19894
mean for supplier B	-7.77246×10^{-2}	15.74048
mean for supplier A	-7.95940×10^{-2}	15.28261
mean for supplier D*	-7.06491×10^{-2}	16.19574
(1) mean for 8 elements from suppliers B and A	-7.86593×10^{-2}	15.51155
estimate of standard deviation for 8 elements from suppliers B and A	0.52891×10^{-2}	
estimate of standard deviation of the mean	0.18700×10^{-2}	
(2) element K2 of reference 9	-8.12993×10^{-2}	16.03712
$\frac{(1)}{(2)}$	0.96753	0.96723

* excluded from mean.

Table A-12. Room Temperature Calibration Parameters, a and b, for Elements Calibrated on September 27, 1975. ($\ln R = a + b\,RH$).

Element-Supplier	b	a
A1 - B	-9.01400×10^{-2}	16.58506
A2 - B	-7.95223×10^{-2}	16.80703
C3 - B	-7.18793×10^{-2}	14.98036
III1 - A	-8.01244×10^{-2}	14.90439
III2 - A	-8.41959×10^{-2}	15.39848
III3 - A	-8.76682×10^{-2}	15.77972
III4 - A	-8.48811×10^{-2}	15.53159
mean for supplier B	-8.05139×10^{-2}	16.12415
mean for supplier A	-8.42174×10^{-2}	15.40354
(1) mean for 7 elements	-8.26302×10^{-2}	15.71238
estimate of standard deviation for 7 elements	0.60665×10^{-2}	
estimate of standard deviation of the mean for 7 elements	0.22929×10^{-2}	
(2) element K2 of reference 9	-8.12993×10^{-2}	16.03712
$\frac{(1)}{(2)}$	1.01637	0.97975

Table A-13. Room Temperature Calibration Parameters, a and b, for Elements from Supplier E Calibrated on April 26, 1976. ($\ln R = a + b\ RH$).

Element	b	a
III1 - E	-10.32980×10^{-2}	17.58000
III4 - E	-10.12638×10^{-2}	17.17377
III2 - E	-13.21357×10^{-2}	19.15191
Element K2 of reference 9	$-\ 8.12993 \times 10^{-2}$	16.03712

NBS-114A (REV. 7-73)

U.S. DEPT. OF COMM. BIBLIOGRAPHIC DATA SHEET	1. PUBLICATION OR REPORT NO. NBSIR 76-1108	2. Gov't Accession No.	3. Recipient's Accession No.

4. TITLE AND SUBTITLE
Fabrication of the Barium Fluoride Film Humidity Sensor by Industrial Firms

5. Publication Date: August 1976

6. Performing Organization Code

7. AUTHOR(S): Frank E. Jones

8. Performing Organ. Report No. NBSIR 76-1108

9. PERFORMING ORGANIZATION NAME AND ADDRESS

NATIONAL BUREAU OF STANDARDS
DEPARTMENT OF COMMERCE
WASHINGTON, D.C. 20234

10. Project/Task/Work Unit No. 2216161

11. Contract/Grant No.

12. Sponsoring Organization Name and Complete Address (*Street, City, State, ZIP*)
Cambridge Air Force Geophysical Laboratories
Department of the Air Force
Hanscom Air Force Base
Bedford, Massachusetts 01731

13. Type of Report & Period Covered: Final

14. Sponsoring Agency Code

15. SUPPLEMENTARY NOTES

16. ABSTRACT (*A 200-word or less factual summary of most significant information. If document includes a significant bibliography or literature survey, mention it here.*)

The barium fluoride film electric hygrometer element, which was conceived and developed at the National Bureau of Standards as a fast responding humidity sensor and which has been used in a variety of research applications, has been successfully fabricated by several commercial firms. This successful transfer of technology from the Federal Government to the private sector should assure the availability of the element for general use, including missile climatology and routine radiosonde use. Calibration equations have been developed and the analysis of calibration data has provided insight into the physical processes involved in the functioning of the element.

It has been shown that the conductance - $\frac{p}{p_s}$ isotherm (in itself a Type II isotherm in the Brunauer designation of physical adsorption isotherms) is a composite of a Type I and two Type III isotherms. The two Type III isotherm isotherm equations are of the form of the Freundlich isotherm equation. These results represent the solution of a long-standing problem in adsorption and have general application to other adsorption systems in addition to the water vapor-barium fluoride film system.

17. KEY WORDS (*six to twelve entries; alphabetical order, capitalize only the first letter of the first key word unless a proper name; separated by semicolons*)
Barium fluoride; calibration equations; fast response; films; humidity sensor; industrial fabrication; isotherm equations; physical adsorption; relative humidity; routine radiosonde application.

18. AVAILABILITY: X Unlimited

For Official Distribution. Do Not Release to NTIS

Order From Sup. of Doc., U.S. Government Printing Office Washington, D.C. 20402, SD Cat. No. C13

X Order From National Technical Information Service (NTIS) Springfield, Virginia 22151

19. SECURITY CLASS (THIS REPORT)	21. NO. OF PAGES
UNCLASSIFIED	73
20. SECURITY CLASS (THIS PAGE)	22. Price
UNCLASSIFIED	$4.50

USCOMM-DC 29042-P74